Czech Technical University in Prague
Faculty of Nuclear Sciences and Physical Engineering

Department of Physics
Experimental Nuclear and Particle Physics

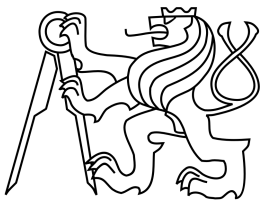

Study of saturation effects in hadrons using Balitsky-Kovchegov evolution equation

RESEARCH THESIS

Author: Marek Matas
Supervisor: Ing. Jan Čepila, Ph.D.
Year: 2015

Před svázáním místo téhle stránky vložíte zadání práce s podpisem děkana (bude to jediný oboustranný list ve Vaší práci) !!!!

Statement

I hereby claim that I have carried out all the academic endeavours honestly and I have used only literature that is listed in the Bibliography attachment.

In Prague .....

.....
Marek Matas

Acknowledgement

I would like to thank Ing. Jan Čepila, Ph.D. for his help with understanding the topic and for supervising my work.

Marek Matas

Author: Marek Matas

Type of work: Research thesis

Supervisor: Ing. Jan Čepila, Ph.D.
FJFI, CTU

Title:
Study of saturation effects in hadrons using Balitsky-Kovchegov evolution equation

Author: Marek Matas

Abstract: Large amount of experimental data mainly from deep inelastic scattering experiments at small Bjorken x allows to test the high energy limit of QCD. It is known that hadron structure functions show large increase of the number of gluons in this limit. This gluon evolution is described by the BFKL evolution equation. However, experimental data suggests that there are less gluons in a hadron then there should be according to the solution of the BFKL equation. This deviation can be due to parton saturation. According to this phenomenon the number of gluons in a hadron is given by the difference by the radiation and recombination processes which leads to dynamically generated balance in the number of gluons driven by the saturation scale. These non-linear effects in hadrons are described by the Balitsky-Kovchegov evolution equation (BK). Solution of the BK is particularly important in the heavy-ion physics.

Key words: Deep Inelastic Scattering, Balitsky-Kovchegov equation, HERA

Název práce:
Studium saturačních efektů v hadronech s použitím Balitski-Kovchegovy evoluční rovnice

Autor: Marek Matas

Abstrakt: Velké množství experimentálních dat, převážně z hluboce nepružného rozptylu s malým Bjorkenovým x umožňuje testovat vysokoenergetickou limitu QCD. Je známo, že hadronové strukturní funkce vykazují nárůst počtu gluonů v této limitě. Tento vývoj je popsán BFKL evoluční rovnicí. Experminetální data ukazují, že v hadronech je méně gluonů, než předpovídá BFKL rovnice. Tato odchylka může být zapříčiněna partonovou saturací. Podle ní je počet gluonů v hadronu dán rozdílem mezi rekombinačními a radiačními procesy, což vede k dynamicky generované rovnováze. Tyto nelineární efekty v hadronech jsou popsány Balitsky-Kovchegovo evoluční rovnicí (BK). Řešení BK rovnice je obzvláště důležité ve fyzice těžkých iontů.

Klíčová slova: Hluboce nepružný rozptyl, Balitsky-Kovchegova rovnice, HERA

Contents

Introduction

There are many experiments studying the properties of particles at the high-energetic limit of QCD. Deep Inelastic Scattering (DIS) studied at HERA experiment is a good tool for measuring such properties. Evolution equations such as BFKL, BK, JMWLK and DGLAP are used to describe the properties of particles that take part in the high energy collisions. The BFKL evolution equation predicts emergence of new partons as the energy of the collision increases and in this approach, the gluon density is not bound by unitarity restrictions.

In the experiments on large accelerators such as HERA or LHC, it was shown that the number of partons does not completely satisfy this equation and that there is less partons then predicted. Measured cross sections predicted by these evolution equations grow above the experimentally obtained values at high energies, where most contribution to the cross section is due to newly created gluons. The effect of number reduction observed in experiment may be due to recombination processes inside the hadrons and it is included in the BK evolution equation. Recombination processes take place when it is not anymore energetically favorable for a new parton to emerge in the hadron and its entire phase space is already populated.

The BK evolution equation is an integro-differential equation and there are several ways to solve it numerically [22, 23, 24]. The BK evolution equation considered in this work includes running coupling kernel that takes into account the two loop processes and assumes impact parameter independent solution [11].

Using numerical methods such as Runge Kutta method of fourth order and Simpson rule, one can obtain the structure functions and reduced cross sections of DIS that account for the recombination processes within the hadron. Numerical methods used to compute these values need to be studied and an optimal setup regarding the precision and speed of computation has to be tested.

Results obtained by solving this equation can be used in describing and understanding processes that occur in heavy-ion physics, especially on experiments such as LHC or RHIC. The obtained solution was then confronted with data from HERA.

Chapter 1

High energy collision phenomenology

1.1 Deep Inelastic Scattering

Deep Inelastic Scattering (DIS) is one of the important tools that allow us to verify physical theories. It is a highly energetic scattering of a lepton off a hadron, where many new particles are created upon the collision and the original hadron falls apart. Such collision can be simplified in a way shown on Fig. 1.1.

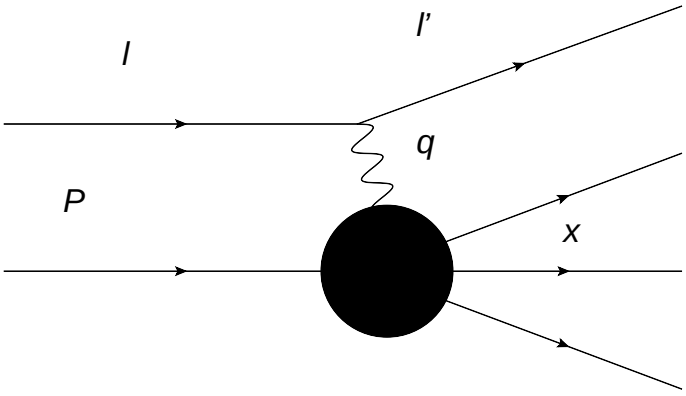

Figure 1.1: Deep inelastic scattering [1].

Equation 1.1. describes such scattering where L is an incoming lepton with four-momentum l, N is a hadron with four-momentum P, L' is the outgoing lepton with four-momentum l' and X represents particles created by the interaction with four-momentum x.

$$L(l) + N(P) \rightarrow L'(l') + X(x) \tag{1.1}$$

1.1.1 Lorentz-invariant variables

To describe this process we need to define Lorentz-invariant variables as shown in Eq. 1.2, 1.3, 1.4 and 1.5. In Eq. 1.2, s is the total energy of the collision in the center of mass (CMS) frame, Q^2 is so called scale of the virtual photon, q^2 is squared four-momentum passed from the lepton to the hadron, ν is the total energy that is passed from the lepton to the target in targets rest frame and x is so called Bjorken x that (in the infinite momentum frame) gives us the ratio of the momentum carried by the scattered gluon or quark to the total momentum carried by the target.

$$s = (P + l)^2 \tag{1.2}$$

$$q^2 = -Q^2 = (l - l')^2 \tag{1.3}$$

$$\nu = \frac{Pq}{m_p} = \frac{W^2 - Q^2 - m_p^2}{2m_p} \tag{1.4}$$

$$x = \frac{AQ^2}{2Pq} = \frac{AQ^2}{Q^2 + W^2 - m_p^2} \tag{1.5}$$

Here m_p is the mass of the proton. We could also define variable W^2, which gives us the total energy that is given to the hadron in the CMS frame as shown in Eq. 1.6

$$W^2 = (P + q)^2 \tag{1.6}$$

$$y = \frac{Pq}{Pl} = \frac{Q^2}{x(s - m_p^2)} \tag{1.7}$$

and equation 1.7 represents the transferred energy fraction. The scale Q^2 defines a resolution of the scattering process, since the incoming particle can interact with objects with size proportional to $1/Q^2$. The bigger Q^2, the better resolution we get. By increasing the energy, we are able to see softer gluons (with smaller fraction of momenta) that are emitted by more energetic gluons.

1.1.2 DIS in infinite momentum frame

The emission of a photon from the lepton is an understood process and is very well described by the Quantum Field Theory. Point-like lepton here in this experiment serves as a source of the virtual photon, that will then interact with the hadron. Scattering of the virtual photon off the hadron results in breaking the hadron and creating other particles. In this model, we are working in the infinite momentum frame which supposes very high momentum of the scattered proton.

If we use the high energy limit and keep Q^2 fixed, the Bjorken x decreases since $s \sim Q^2/x$. Therefore, the observed objects carry lower and lower fraction of the total momentum. In the high energy region, proton is mostly populated by gluons

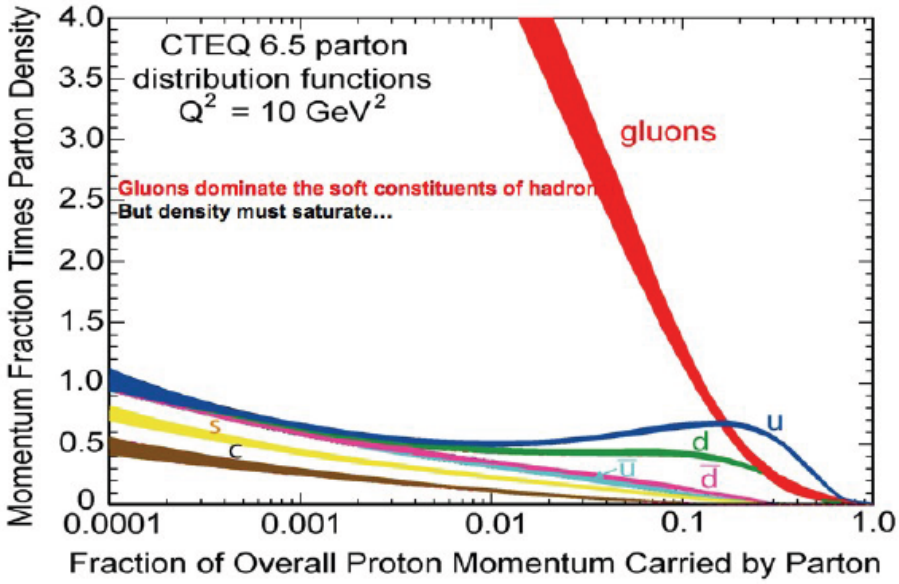

Figure 1.2: Distribution of parton density for different constituents of a proton [4].

(which is explained more further in the thesis) [17, 18, 19] and therefore we will neglect the effects of quarks as shown in fig 1.2. In this figure we can see how the parton density distribution evolves for different partons with respect to Bjorken x. We can see that below $x \sim 10^{-1}$, gluons carry most momenta and that this density grows above all boundaries. This will be fixed by the introduction of saturation effects in the following sections.

The differential cross section depends on energy and scale of the process. The equation 1.8 shows such dependence, where $F_1(x, Q^2)$ and $F_2(x, Q^2)$ are the structure functions of proton, α represents the electromagnetic coupling, y is the inelasticity, x is the Bjorken x and Q^2 is the scale of the virtual photon.

$$\begin{aligned} \frac{d^2\sigma}{dxdQ^2} &= \frac{4\pi\alpha^2}{xQ^4}((1-y)F_2 + y^2 x F_1) \\ &= \frac{4\pi\alpha^2}{xQ^4}\left(\left(1 - y + \frac{y^2}{2}\right)F_2 - \frac{y^2}{2}F_L\right) \end{aligned} \tag{1.8}$$

because

$$F_L = F_2 - 2xF_1 \tag{1.9}$$

where F_L is called the longitudinal structure function.

For the structure functions $F_L(x, Q^2)$ and $F_2(x, Q^2)$ stands

$$F_2 = \frac{Q^2(1-x)}{4\pi^2\alpha}\frac{Q^2}{Q^2 + 4m_p^2x^2}\sigma_{tot}^{\gamma^* p} \tag{1.10}$$

$$F_L = \frac{Q^2(1-x)}{4\pi^2\alpha}\sigma_L \tag{1.11}$$

which with the approximation of $x \to 0$ changes into

$$F_2 = \frac{Q^2(1-x)}{4\pi^2\alpha}(\sigma_T + \sigma_L) \tag{1.12}$$

$$F_L = \frac{Q^2}{4\pi^2\alpha}\sigma_L \tag{1.13}$$

[15] since for $\sigma_{tot}^{\gamma * p}$ stands

$$\sigma_{tot}^{\gamma * p} = \sigma_T + \sigma_L \tag{1.14}$$

where σ_T and σ_L are the cross sections for absorption of longitudinally and transversally polarized photons and m_p is the mass of a proton.

The structure function $F_2(x, Q^2)$ can be also expressed using parton model as

$$F_2(x, Q^2) = x \sum_i e_{q_i}^2 (q_i(x, Q^2) + \bar{q}_i(x, Q^2)) \tag{1.15}$$

where q_i is the quark density, $\bar{q}_i$ the antiquark density, e_{q_i} is the charge of the quark divided by the unit charge and the sum runs over all quark flavors.

Similarly, the longitudinal structure function can be expressed as [11]

$$F_L(x, Q^2) = \frac{\alpha_s}{4\pi} x^2 \int_x^1 \frac{dz}{z^3} \left(\frac{16}{3} F_2(x, Q^2 \right) + 8 \sum_i e_{q_i}^2 \left(1 - \frac{x}{z}\right) z g(z, Q^2) \tag{1.16}$$

In the low x region, the gluon density term will be dominant.

1.1.3 Color dipole approach to DIS

So far we have assumed the infinite momentum frame of the collision and we have shown how the inner composition of proton changes with respect to energy and scale of the incoming photon.

If we consider target rest frame, the lepton - hadron collision is as follows. First, the incoming lepton emits a virtual photon. This photon then spontaneously fluctuates into a quark - antiquark color dipole (analogy to the dipole in electrodynamics). This dipole then interacts strongly with the target proton and its further fluctuation back into a photon is disrupted. The fluctuation of a photon into the color dipole is necessary because of new particles that emerge from the collision, which is only

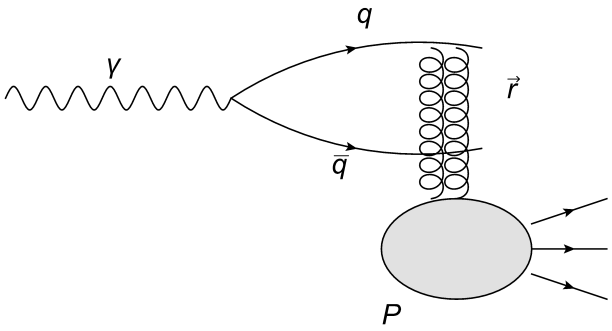

Figure 1.3: Color dipole fluctuating from the virtual photon [2].

possible when strong interaction is present and could not be described by mere electromagnetic interaction.

At small x, it can be shown that the lifetime of such quark - antiquark fluctuation is greater than the average time of the whole interaction [1], which is important because then the dipole has enough time to react with the target hadron before it annihilates. The cross section of the total photon-proton scattering is shown in 1.17, where $\mid \Psi^i_{T,L} \mid^2$ is the wave function of the photon that fluctuates to create a color dipole. Indexes T and L correspond to transverse and longitudinal polarizations of the incident photon and e_{q_i}, m_{q_i} and z correspond to fractional electric charge of quark q_i, its mass and fraction of the longitudinal momentum of photon it carries.

$$\sigma^{\gamma^* - h}_{T,L}(x, Q^2) = \sum_i \int_0^1 dz \int d\vec{r} \mid \Psi^i_{T,L}(e_{q_i}, m_{q_i}, z, Q^2, \vec{r}) \mid^2 \sigma^{q\bar{q}}(\vec{r}, x) \tag{1.17}$$

The final cross section is then computed by integrating the photon-color dipole wavefunction and the cross section of the quark-antiquark dipole scattering of the proton target over all transverse dipole sizes $\vec{r}$ and over all possible values of photon's fractional momentum z.

Using dipole cross-section $\sigma^{q\bar{q}}(r, x)$ we can compute the structure function F_2 that can be measured experimentally as shown in Eq. 1.18

$$F_2(x, Q^2) = \frac{Q^2}{4\pi^2 \alpha_{em}} \int d\vec{r} dz \mid \Psi^i_{T,L}(z, \vec{r}) \mid^2 \sigma^{q\bar{q}}(\vec{r}, \tilde{x}) \tag{1.18}$$

Where $\mid \Psi^i_{T,L}(z, \vec{r}) \mid^2$ is a sum of squared longitudinal and transversal photon wave functions as shown in Eq. 1.20 and $\tilde{x}$ is introduced due to photoproduction limit as shown in Eq. 1.19 [12].

$$\tilde{x} = x \left(1 + \frac{4m^2_{q_i}}{Q^2}\right) \tag{1.19}$$

where the mass of the incident quark is set to the value of $140\,\mathrm{MeV/c^2}$.

$$\mid \Psi^f_{T,L}(z,\vec{r}) \mid^2 = \mid \Psi^i_T(z,\vec{r})^2 \mid + \mid \Psi^i_L(z,\vec{r})^2 \mid \tag{1.20}$$

and the longitudinal and transversal photon wave functions are given by

$$\mid \Psi^i_T(z,\vec{r},Q^2)^2 \mid = \frac{3\alpha_{em}}{2\pi^2} \sum_f e^2_{q_i}((z^2+(1-z)^2)\epsilon^2 K_1^2(\epsilon r) + m^2_{q_i} K_0^2(\epsilon r)) \tag{1.21}$$

$$\mid \Psi^i_L(z,\vec{r},Q^2)^2 \mid = \frac{3\alpha_{em}}{2\pi^2} \sum_f e^2_{q_i}(4Q^2 z^2 (1-z)^2 K_0^2(\epsilon r)) \tag{1.22}$$

where z is the fraction of the total momentum carried by the quark, K_0 and K_1 are the MacDonald functions.

$$\epsilon^2 = z(1-z)Q^2 + m^2_{q_i} \tag{1.23}$$

The actual dipole scattering cross section is then computed by integrating the dipole-proton scattering amplitude over the impact parameter as shown in Eq. 1.24.

$$\sigma^{q\bar{q}}(r,x) = 2\int d\vec{b} N(x,r,\vec{b}) \tag{1.24}$$

This dipole cross section then covers all the QCD effects and can be also obtained from the BK evolution equation. If we neglect the dependence of the scattering amplitude N on the impact parameter, the integral over it can be simplified into expression 1.25. [5],

$$\sigma^{q\bar{q}}(r,x) = \sigma_0 N(x,r) \tag{1.25}$$

where σ_0 is a parameter that we fit from data.

m_{q_i} is the mass of the considered quark. The data obtained from HERA suggests that the assumption of independence of the scattering amplitude N to the impact parameter is valid. This assumption corresponds to approximating the target with finitely big homogeneous hadron where the size of this hadron is fitted to measured data. The scattering amplitude reaches values between 1 and 0. As the Bjorken x decreases (energy increases) the number of gluons grows and the scattering amplitude approaches 1 since it is very probable for the dipole to interact with this dense hadron. Its value also increases towards one with the increase of dipole distance r. With the limit $r \to 0$, we get $N \to 0$ due to the color transparency effect in low r values.

1.2 Evolution equations of parton densities

During the interaction, color dipole exchanges a particle with the target hadron. To maintain the color conservation, the exchanged particle must be colorless and in the

first approximation we consider it to be a pair of two gluons. The actual complex particle that is exchanged is called Pomeron. A linear approach to the interaction such as the one used in BFKL evolution equation suggests only one particle exchange between the color dipole and target hadron where as non-linear evolution equations such as the BK equations suggest multiple pomeron exchanges as shown in Fig. 1.4.

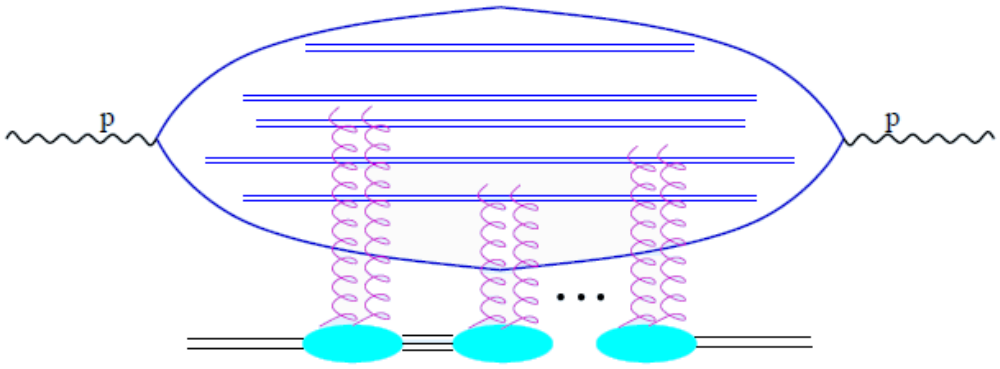

Figure 1.4: Multiple pomeron exchange between the color dipole and the target hadron [3].

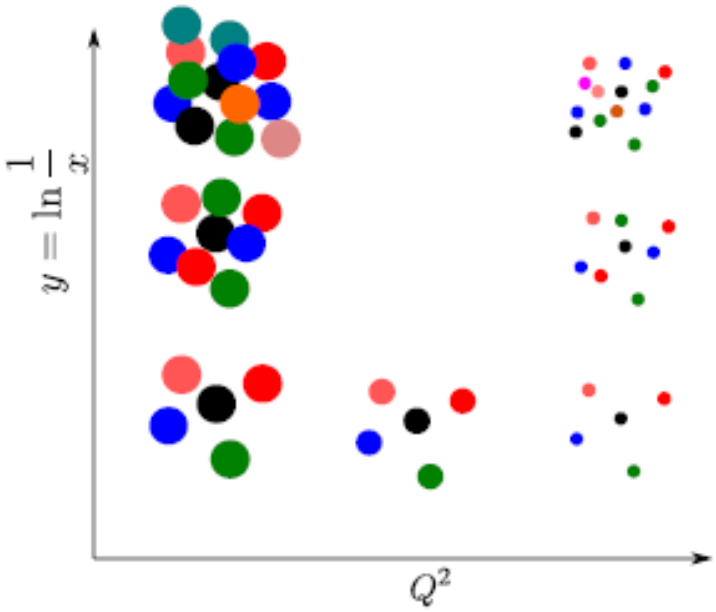

Figure 1.5: Gluon number and size with respect to rapidity and scale [1].

If we fix the scale of the virtual photon and increase the energy of the collision, we observe that some gluons start to overlap due to fixed dimensions of the proton itself. In this case we have to take into account the recombination processes that take place among gluons as they become more influential. The scale when gluons start to overlap is called saturation scale and occurs when most of the space in the proton

is already occupied by other gluons. Further decreasing of Bjorken x will then not result into further gluon number rise since the whole system is already saturated and the new gluons are compensated with the recombination processes and a dynamical balance is established. This situation varies for different scales as with higher Q^2, we decrease the dimensions of the gluons itself. We can determine a so called saturation scale Q_s at which this effect takes place with respect to the total energy. These non-linear recombination processes are described by the Balitsky-Kovchegov evolution equation (BK).

1.2.1 The DGLAP equations

The DGLAP (Dokshitzer-Gribov-Lipatov-Altarelli-Parisi) equations are usually used in interactions, where Q^2 is large and x is not too small [11]. They describe the change of parton size when bigger and bigger scale is introduced. The equations itself stand:

$$\frac{dg(x,Q^2)}{dlnQ^2} = \frac{\alpha_s}{2\pi}\int_x^1 \frac{dz}{z}\left(\sum_i q_i(z,Q^2)P_{gq}\left(\frac{x}{z}\right) + g(x,Q^2)P_{gg}\left(\frac{x}{z}\right)\right) \tag{1.26}$$

and

$$\frac{dq_i(x,Q^2)}{dlnQ^2} = \frac{\alpha_s}{2\pi}\int_x^1 \frac{dz}{z}\left(q_i(z,Q^2)P_{qq}\left(\frac{x}{z}\right) + g(x,Q^2)P_{qg}\left(\frac{x}{z}\right)\right) \tag{1.27}$$

where q_i is the quark density for the flavor i and g is the gluon density. $P_{ij}(a)$ are the Altarelli-Parisi splitting functions given by terms

$$\begin{aligned}
P_{qq}(a) &= \frac{4}{3}\frac{1+a^2}{1-a} = P_{gq}(1-a)\\
P_{gq}(a) &= \frac{4}{3}\frac{1+(1-a)^2}{a} = P_{qq}(1-a)\\
P_{qg}(a) &= \frac{1}{2}(a^2+(1-a)^2) = P_{qg}(1-a)\\
P_{gg}(a) &= 6\left(\frac{a}{1-a}+\frac{1-a}{a}+a(1-a)\right) = P_{gg}(1-a)
\end{aligned} \tag{1.28}$$

x is the Bjorken x, α_s is the strong coupling constant and Q^2 is the scale of the virtual photon. These equations tell us how the structure functions change when different scale is introduced.

1.2.2 The BFKL evolution equation

The BFKL (Balitsky-Fadin-Kuraev-Lipatov) evolution equation holds validity in the region where Q^2 is finite and x is low [11], namely

$$\alpha_s(Q^2) ln \frac{Q^2}{Q_0^2} \ll \alpha_s(Q^2) ln \frac{1}{x} < 1 \tag{1.29}$$

In the BFKL equation, the unintegrated gluon density $f(x, k_T^2)$ is used and from that we can obtain the actual gluon density by using the formula

$$xg(x, Q^2) = \int_0^{Q^2} \frac{d\vec{k_T}}{k_T^2} f(x, k_T^2). \tag{1.30}$$

Note that $\vec{k_T}$ is the transverse momentum of the emitted gluon. The BFKL equation then stands as

$$\frac{\partial f(x, k_T^2)}{\partial ln(1/x)} = \frac{3\alpha_s}{\pi} k_T^2 \int_0^{\infty} \frac{d\vec{k_T'}}{k_T'^2} \left(\frac{f(x, k_T'^2) - f(x, k_T^2)}{| k_T'^2 - k_T^2 |} + \frac{f(x, k_T'^2)}{\sqrt{4k_T'^4 + k_T^4}} \right). \tag{1.31}$$

As the color dipole is accelerated, one of the quarks in the quark-antiquark dipole can also emit gluons as shown on Fig. 1.6. These gluons can then emit further gluons and some of these gluons may fluctuate into other quark-antiquark dipoles within the original dipole created by the virtual photon. These dipoles do not interact with each other and many are created within the original dipole, creating a complicated structure.

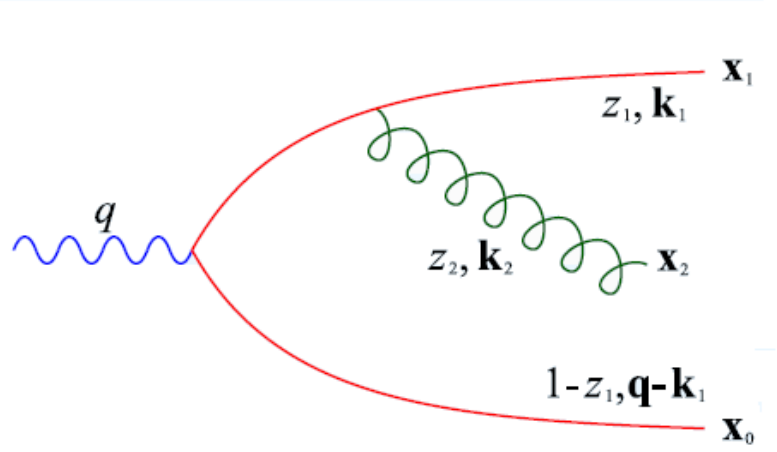

Figure 1.6: Color dipole that emits another gluon [3].

1.3 Color Glass Condensate and saturation

Color Glass Condensate (CGC) describes a high energy limit state of hadrons. It is a very densely packed state filled with interacting gluons. This state is the starting state in hadron collisions that are schematically shown in Fig. 1.7.

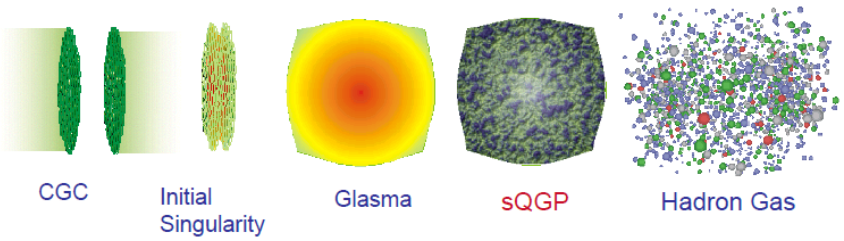

Figure 1.7: Different phases in hadron collision [4].

In this picture we see on the left side two particles in their CGC state just before the collision. At the exact time of collision, initial singularity is formed from which all the following states will emerge (it is not an actual geometrical singularity). First, Glasma is formed, which is a short-living precursor the Quark Gluon Plasma (QGP). Its name is derived from the very hot and dense amorphous packing of gluons somewhat similar to the structure of metallic glasses and other amorphous structures. After a short period of time, Quark Gluon Plasma is formed that later evolves into the free hadron gas.

In the low energetic limit, collisions and new particle creation is dominated by the quarks, quark antiquark pairs and a few gluons. As $x \to 0$, gluons dominate the collision and they are most responsible for the new particle creation.

Since at low Bjorken x there is high density of small gluons, a strong self interaction occurs. Due to the very dense packing and asymptotic freedom of QCD, the interaction between gluons will be weak for the individual gluons but can prove to be strong in general due to its coherent properties. The whole proton will be filled with gluons when the gluon density will be in order of $\frac{1}{\alpha_S}$ that is when it will not be anymore energetically favorable for new gluons to be added to the system. If we try to add new gluons, first the soft gluons with low energy and big dimensions will fill the entire phase space of the proton so that it is not favorable for new gluons to emerge. Then only more energetic gluons that have a smaller dimensions can be added to the system. Note that we are considering only dimensions connected with the transverse momentum plane and therefore corresponding with the transverse momentum distribution.

It means that with a fixed energy of a proton, its volume is filled with gluons of dimensions that correspond to energy and if we wanted to add more gluons to the system, we would have to increase the energy since only gluons with higher p_T are energetically favorable to be added to the system. For every Bjorken x of the hadron, there is a certain saturation transverse momentum and below that momentum the whole phase space is saturated. This is schematically shown in Fig. 1.8.

That is why this structure is called a Color Glass Condensate. Color, because it is composed of particles with a color charge, Glass because it evolves slowly compared to its environment and Condensate because all the phase space of such CGC is filled with gluons until the saturation scale is reached. The whole hadron is Lorentz contracted due to its high momentum and the distribution of the color fields within

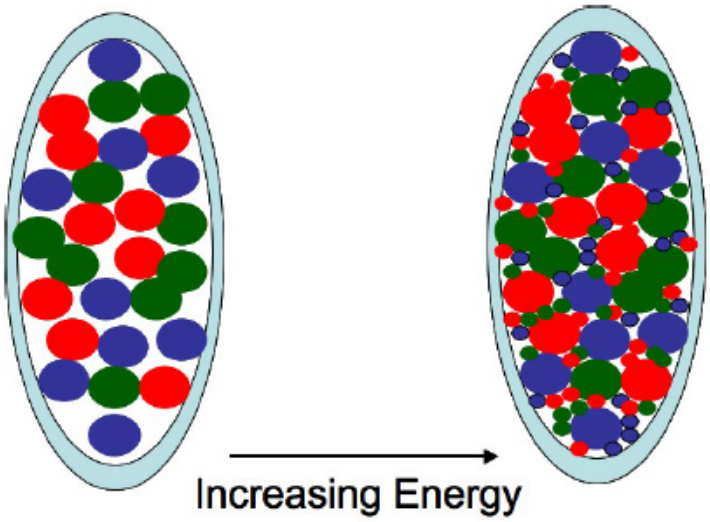

Figure 1.8: Saturation of proton by new high energetic (small) gluons [4].

it is randomly polarized with random color. The gluon fields inside CGC correspond to a low x (high energy) and its sources correspond to high Bjorken x [4]. The CGC model predicts that gluons with low Bjorken x will never saturate as we can always lower its x correspondingly to the saturation scale.

The CGC model is proven to describe well high energetic hadrons with x corresponding to 10^{-2}. Without the introduction of saturation to the QCD models, the cross section of gluon interaction diverges as x decreases at a rate of $\frac{1}{p_T^4}$.

1.3.1 The JIMWLK equations

The JIMWLK evolution equations [25, 26, 27, 28, 29, 30] is a more general expression that with approximation of large N_c limit reduces to the BK evolution equation. However when the computation is made and compared with the approximated BK evolution equation, we get only about 0.01 difference between the two results, which is much less than the values expected [10]. The JIMWLK equations are not integro-differential equations such as BK but a set of functional differential equations given by following expressions.

$$\frac{\partial W_Y[\alpha]}{\partial Y} = H W_Y[\alpha] \tag{1.32}$$

$W_Y[\alpha]$ is the functional probability distribution. This distribution describes the behavior of color sources with changing rapidity and H is the Hamiltonian of the JIMWLK equation given by

$$H = -\frac{1}{16\pi^3}\int_{uvz} M_{uvz}\left(1 + V_u^\dagger V_v - V_u^\dagger V_z - V_z^\dagger V_v\right)^{ab}\frac{\delta}{\delta\alpha_u^a}\frac{\delta}{\delta\alpha_v^b}, \tag{1.33}$$

here α_u^a is a gauge invariant functional. The notation for the integral follows $\int_{u..} = \int du^2$ and M is the kernel given by expression

$$M^{uvz} = \frac{(u-v)^2}{(u-z)^2(z-v)^2}. \tag{1.34}$$

$V_x^\dagger$ and V_x are Wilson lines given by

$$V_x^\dagger = P\exp\{ig\int_{-\infty}^{\infty} dz^- \alpha_a(z_-, x)\} \tag{1.35}$$

where P denotes that the z^- is path-ordered [32].

1.3.2 Balitsky-Kovchegov evolution equation

Balitsky-Kovchegov evolution equation (BK) is one of the equations that describe the evolution of the scattering amplitude N. It was derived from the JIMWLK evolution equations in the limit of large number of colors by Kovchegov [20, 21]. It is a modification of BKFL evolution equation and unlike BFKL, does account for the nonlinear effects of gluon recombination. The BK evolution equation is shown in 1.36 [13].

$$\frac{\partial N(r,x)}{\partial Y} = \int d\vec{r_1} K^{run}(\vec{r},\vec{r_1},\vec{r_2})(N(\vec{r_1},x) + N(\vec{r_2},x) - N(\vec{r},x) - N(\vec{r_1},x)N(\vec{r_2},x)) \tag{1.36}$$

Where $K^{run}(\vec{r},\vec{r_1},\vec{r_2})$ can be expressed as in Eq. 1.37 [14].

$$K^{run}(\vec{r},\vec{r_1},\vec{r_2}) = \frac{N_c\alpha_s(r^2)}{2\pi^2}\left(\frac{r^2}{r_1^2 r_2^2} + \frac{1}{r_1^2}\left(\frac{\alpha_s(r_1^2)}{\alpha_s(r_2^2)} - 1\right) + \frac{1}{r_2^2}\left(\frac{\alpha_s(r_2^2)}{\alpha_s(r_1^2)} - 1\right)\right) \tag{1.37}$$

and $\vec{r_2} = \vec{r} - \vec{r_1}$. If we disregard the last term in the BK equation, we obtain a linear equation that can be shown to be equivalent to the BFKL evolution equation [3]. This linear version does not involve the recombination processes and therefore is not accurate for very small Bjorken x. As the rapidity increases, this linearized version rises the scattering amplitude above any boundary and the comparison to the BK equation is shown in Fig. 1.9.

QCD perturbative theory is only applicable for high energies, where the coupling constant is significantly low. In the low energy region, a non-perturbative approach is necessary. This would correspond to a low x strip along the y-axis in Fig. 1.10.

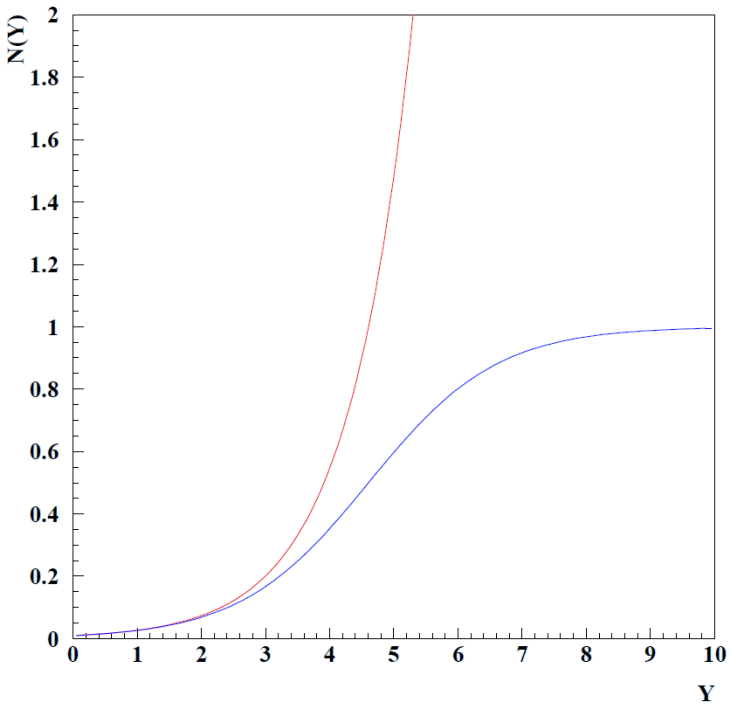

Figure 1.9: Comparison of the BK equation solutions (blue line) to the BFKL equation solutions (red line) [3].

Below the saturation scale, BFKL and other linear equation are valid and above this line we get dense and energetic systems described by the BK equation. This area of validity is shown in Fig. 1.10.

The coupling that is used in the kernel of the integro-differential equation depends on the number of considered quark flavors according to equation 1.38.

$$\alpha_{s,n_f}(r^2) = \frac{4\pi}{\beta_{0,n_f} ln\left(\frac{4C^2}{r^2\Lambda^2_{n_f}}\right)}, \tag{1.38}$$

where

$$\beta_{0,n_f} = 11 - \frac{2}{3}n_f. \tag{1.39}$$

The constant C^2 is the uncertainty coming from the Fourier transformation that was used to derive this result and is usually fit by the data [5]. The constant n_f corresponds to the number of flavors that are active, and is usually set to a value of 3 in the light flavor quarks approximation. $\Lambda^2_{n_f}$ is called the QCD scale parameter and its value depends on the value of n_f. Since all dipole sizes are accounted for in the BK evolution equation, there is a need to reduce the coupling after a certain value is reached, so that the maximal value of coupling constant would not exceed a

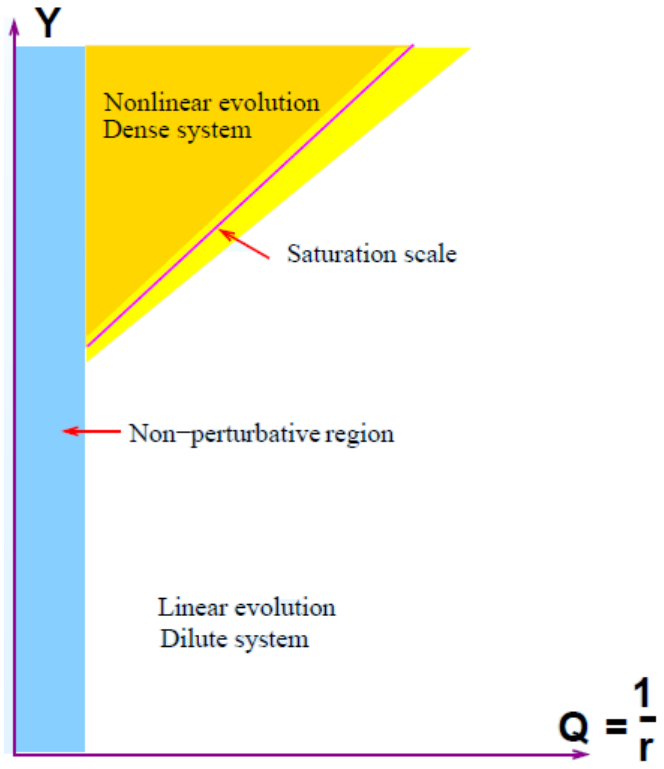

Figure 1.10: A schematic area distribution of validity for different evolution equations [3].

set limit [5]. This modified coupling is called running coupling and takes into account the next to leading two loop expressions [11].

In order to compute the Balitsky Kovchegov evolution equation and get the cross section of the whole interaction or a structure function of a hadron, one must start with certain initial conditions. One of the frequently used initial conditions is the GBW initial condition Eq. 1.40 [5].

$$N^{GBW}(r, x = x_0) = 1 - exp\left(-\frac{(r^2 Q_{s0}^2)^\gamma}{4}\right) \tag{1.40}$$

Another typical initial condition for the BK equation is a MV initial condition 1.41 [16]

$$N^{MV}(r, x = x_0) = 1 - exp\left(-\frac{(r^2 Q_{s0}^2)^\gamma}{4} ln\left(\frac{1}{r\Lambda} + e\right)\right) \tag{1.41}$$

Where Λ represents the infrared cutoff of the dipole cross section and does not have to be equal to $\Lambda_{n_f}^2$ introduced earlier [5], Q_{s0}^2 is the scale for the biggest Bjorken x that is considered in the computation and γ is a parameter that controls the slope of the fall of the dipole amplitude when r is decreased. Solutions of the BK equation even seem very similar with the same shape, only shifted with rapidity evolution. However the BK evolution equation does not include the quantum fluctuations of the

fit	Q_{s0}^2	C	$\Lambda_{n_f}^2$	γ	σ_0
GBW	0.241	2.46	0.241	0.971	32.357
MV	0.165	$\sqrt{6.5}$	0.241	1.13	32.895

Table 1.1: A possible values of the initial condition parameters.

gluon field and therefore its saturation scale is not entirely accurate. The fluctuations are not accounted for in the fixed coupling approach. The running coupling approach shown in Eq. 1.38 evens its effects out [3]. Table 1.3.2 shows possible values for the initial parameters.

1.4 HERA description

HERA is an accelerator with center of mass energy reaching up to 300 GeV located in Germany, it is the first electron-proton collider in the world [11]. Its high energy limit allows us to study the structure of proton up to the limit of 10^{-18} m and partons with very low Bjorken x. In the $p-e$ interactions, p is a strongly interacting particle incoming to the collision itself which gives us additional tools and possibilities for studying perturbative QCD, jet physics and the development of strong coupling α_s when compared to lepton-lepton scattering.

The circumference of the circular accelerator is 6.3 km. The electron and proton beams propagate in separate rings and collide in two sites, where the ZEUS and H1 experiments are placed. The average peak luminosity was measured to be $8.4 \cdot 10^{30} cm^{-2} s^{-1}$. The H1 detector is specialized to measure and tract the outgoing electron and the ZEUS detector specializes in detecting the hadronic showers.

The Lorentz-invariant variables can be obtained from such measurement by measuring the lepton only or from the hadronic system. The way to get the transferred energy fraction and scale for both cases is shown in following equations.

$$y_e = 1 - \frac{E'_e}{E_e} sin^2 \frac{\theta_e}{2} \tag{1.42}$$

$$Q_e^2 = 4 E'_e E_e cos^2 \frac{\theta_e}{2} \tag{1.43}$$

Where E_e, E'_e is the electron energy before and after the collision and θ_e is the angle of the scattered electron with respect to the proton trajectory. The index e represents the electron method and h represents the hadron method.

$$y_h = \frac{E_H - p_{zH}}{2E_e} \tag{1.44}$$

$$Q_h^2 = \frac{p_{xH}^2 + p_{yH}^2}{1 - y_h} \tag{1.45}$$

Here the E_H, p_{zH}, p_{xH} and p_{yH} are four vectors describing the hadronic system.

Chapter 2

Numerical methods

2.1 Runge-Kutta method

Runge-Kutta method is a commonly used method of solving linear differential equations such as 2.1. Let us consider following notation, $y(x)$ is the desired function,

$$y'(x) = f(x, y) \tag{2.1}$$

and the initial condition is

$$y(a) = \varphi \tag{2.2}$$

The next step of this method is calculated as follows [7]

$$K(x, y, h) = w_1 k_1 + w_2 k_2 + w_3 k_3 + ... + w_s k_s \tag{2.3}$$

where

$$k_i = f\left(x + \alpha_i h, y + h \sum_{j=1}^{i-1} \beta_{i,j} k_j\right), i = 2, ..., s. \tag{2.4}$$

where α_i and $\beta_{i,j}$ are constants that we match to the Taylor's expansion as accurate as possible. Solving an equation according to Runge-Kutta method, one must compute the right side of equation 2.1 in multiple points but does not need to make any additional derivatives. The constants $w_1 k_1, w_2 k_2, w_3 k_3, ..., w_s k_s$ fulfill a condition

$$w_1 k_1 + w_2 k_2 + w_3 k_3 ... + w_s k_s = 1 \tag{2.5}$$

but they vary for different orders of Runge-Kutta method. The way a new step in RK method is computed is shown in Eq. 2.6.

$$y_{n+1}(x_{n+1}) = y_n + hK_n(x, y, h) \tag{2.6}$$

2.1.1 First order - Euler Method

Euler method is a way to compute a linear first order differential equation. Strictly speaking, Euler method is a first order Runge-Kutta method. The simplicity of this method comes from the fact that for computation of the next step y_{n+1} one needs to know only the functions behavior on a neighborhood of the coordinate x_n. The Euler method reads:

$$y_{n+1} = y_n + f(x_n, y_n), n = 0, 1, 2...x_n \in < a, b > \tag{2.7}$$

This method is discrete. That means that its solution will be found only in certain selected coordinates x_n where n = 0, 1, 2, 3..., N. Equidistant selection of x_n simplifies the solution and makes it more precise. In this approach we can introduce the integration step of Euler method h as in Eq. 2.8.

$$x_n = a + nh, n = 0, 1, 2... \tag{2.8}$$

an analogous approach to the problem of solving this kind of differential equation would be Picards method which integrates the whole equation 2.1 and then solves it as in Eq. 2.9 [7].

$$y(x) = \varphi + \int_a^x f(t, y(t))dt \tag{2.9}$$

If the right side of the equation 2.1 fulfills the conditions of being defined and continuous for a $a \leq x \leq b$ and $-\infty \leq y \leq \infty$ and if there exists a constant L for which holds

$$\mid f(x, y) - f(x, z) \mid \leq L \mid y - z \mid \tag{2.10}$$

for every $x \in < a, b >$ and for arbitrary y and z, the solution of such equation exists on the whole interval $< a, b >$ [7].

The graphical interpretation of Euler method is simple. The method takes the slope of the desired function at its initial point and linearly interpolates this function to get the next point after the length of integration step h. This process is repeated until the approximated function is obtained.

The total error of the Euler method is not easy to compute and confine because it accumulates as the method continues and depends only on one parameter of this method and that is the integration step h. It is easier to state the local discrete error which states the error of this method after one step assuming that all the previously used values are correct, see Eq. 2.11 [7].

$$L(y(x), h) = y(x + h) - y(x) - hf(x, y(x)) \tag{2.11}$$

The total error is then given by the multiple local errors piling up with the fact that the starting values of next steps are already shifted from the original function. If this accumulation does not reach too high values, the method is said to be stable.

2.1.2 Second order - Ralston method

As an example of the Runge-Kutta method of second order we can take the Ralston method [7]. This method is more accurate then just the simple Euler method because it takes into account the behavior of the function not only on the neighborhood of the x_n but as well on the neighborhood of $x_n + \frac{2}{3}h$. The next step and its coefficients k_1 and k_2 are calculated as follows.

$$\begin{aligned} y_{n+1} &= y_n + h\left(\frac{1}{4}k_1 + \frac{3}{4}k_2\right) \\ k_1 &= f(x_n, y_n) \\ k_2 &= f\left(x_n + \frac{2}{3}h, y_n + \frac{2}{3}hk_1\right) \end{aligned} \tag{2.12}$$

2.1.3 Fourth order

One of the very often used types of Runge-Kutta methods is the Runge-Kutta method of fourth order for which the setup is as shown in Eq. 2.13

$$\begin{aligned} y_{n+1} &= y_n + \frac{1}{6}h(k_1 + 2k_2 + 2k_3 + k_4) \\ k_1 &= f(x_n, y_n) \\ k_2 &= f\left(x_n + \frac{1}{2}h, y_n + \frac{1}{2}hk_1\right) \\ k_3 &= f\left(x_n + \frac{1}{2}h, y_n + \frac{1}{2}hk_2\right) \\ k_4 &= f(x_n + h, y_n + hk_3) \end{aligned} \tag{2.13}$$

This method is by far the most common of the Runge-Kutta methods, so often when referred to RK method without further specification, this particular setup is considered. Similar to the Euler method, to get the total error of the Runge-Kutta method, we need to know the local discrete error for a single step with correct initial parameters.

If in a neighborhood of point (x_n, y_n) holds

$$\mid f(x, y) \mid < M, \left|\frac{\partial_{i+j} f}{\partial x^i \partial y^j}\right| < \frac{L^{i+j}}{M^{j-1}}, i + j \leq p \tag{2.14}$$

then the error of a method of fourth order is [7]

$$\begin{aligned} &\mid L(y(x_n),h) \mid < (16 \mid b_1 \mid +4 \mid b_2 \mid + \mid b_2+3b_3 \mid + \mid 2b_2+3b_3 \mid + \\ &\mid b_2+b_3 \mid + \mid b_3 \mid +8 \mid b_4 \mid + \mid b_5 \mid + \mid 2b_5+b_7 \mid + \mid b_5+b_6+b_7 \mid \\ &+ \mid b_6 \mid + \mid 2b_6+b_7 \mid + \mid b_7 \mid + \mid 2b_8 \mid)h^5ML^4 \end{aligned} \tag{2.15}$$

where the constants b_i, i = 1, 2, 3, 4, 5, 6, 7 are as follows:

$$\begin{aligned} b_1 &= \frac{1}{120} - \frac{1}{2}(\alpha_2^4 w_2 + \alpha_3^4 w_3 + w_4), \\ b_2 &= \frac{1}{20} - \frac{1}{2}(\alpha_2\alpha_3^2\beta_{32}w_3 + (\alpha_2\beta_{42} + \alpha_3\beta_{43})w_4), \\ b_3 &= \frac{1}{120} - \frac{1}{6}(\alpha_2^3\beta_{32}w_3 + (\alpha_2^3\beta_{42} + \alpha_3^3\beta_{43})w_4), \\ b_4 &= \frac{1}{30} - \frac{1}{2}(\alpha_2^2\alpha_3\beta_{32}w_3 + (\alpha_2^2\beta_{42} + \alpha_3^2\beta_{43})w_4), \\ b_5 &= \frac{1}{120} - \frac{1}{2}\alpha_2^2\beta_{32}\beta_{43}w_4, \\ b_6 &= \frac{1}{40} - \frac{1}{2}(\alpha_2^2\beta_{32}w_3 + (\alpha_2\beta_{42} + \alpha_3^2\beta_{43})^2 w_4), \\ b_7 &= \frac{7}{120} - \alpha_2(1+\alpha_3)\beta_{32}\beta_{43}w_4, \\ b_8 &= \frac{1}{120}. \end{aligned} \tag{2.16}$$

For the often used version of Runge-Kutta method of fourth order 2.13,the expression for an error after a single step is

$$\mid L(y(x_n),h) \mid < \frac{73}{720}h^5ML^4 \tag{2.17}$$

where L is a constant. Since this local error is strongly step dependent, it is in principle possible to consider Runge-Kutta methods with variable integration step length, that is chosen in every point on the grid so that the local error is constant everywhere. This can be achieved by the equation 2.18, where computing the local error simultaneously with the main computation in every other step slows the whole program down approximately by 50% [7].

$$\phi(x_n, y(x_n))h^{p+1} = \frac{1}{2^{p+1}-1}(y_{n+1} - y^*_{n+1}) \tag{2.18}$$

where y_{n+1} is a solution with the integration step h at x_{n+1}, y^*_{n+1} is a solution with integration step $2h$ at $x = x_{n-1}$ and p is the order of of the local discrete error. It is the largest integer for which holds that

$$L(y(x); h) = O(h^{p+1}). \tag{2.19}$$

2.2 Simpson method

Simpson method is a numerical way of computing an integral over a function if the values of this integrated function are known over the interval we want to integrate it on. This method is a method composed [7], which means that another method is used for its construction, in this case it is the Newton-Cotes integration formula.

These formulas approximate the integral

$$I(f) = \int_b^a f(x)dx \tag{2.20}$$

by adding values of the integrated function in certain points on the x-axis multiplied by a factor H_i as shown in Eq. 2.21 [7].

$$I_{n+1}(f) = \sum_{i=0}^{n} H_i f(a_i), \tag{2.21}$$

where a_i are distributed in the interval $< a, b >$. The Newton-Cotes integration formula is a method that uses equidistant spacing of these a_i points and values of H_i are chosen so that the order of this method (maximal order of a polynomial that is integrated without error) is maximal.

Simpson method divides the interval $< a, b >$ into $m/2$ subintervals $< a_{2i}, a_{2i+2} >$ where i = 0,1,2...$m/2$ - 1, and uses the closed Newton-Cotes formula on each one of them separately. The approximate integral is then given by the Eq. 2.22 [7].

$$\begin{aligned}\int_b^b f(x)dx =& \frac{h}{3}(f(a_0) + 4f(a_1) + 2f(a_2) + 4f(a_3) + ... + 4f(a_{m-3}) \\ &+ 2f(a_{m-2}) + 4f(a_{m-1}) + f(a_m)) + E(f),\end{aligned} \tag{2.22}$$

where h is the integration step given by $h = \frac{(b-a)}{m}$, m is an even integer and $E(f)$ is the error of the method given by [7]

$$E(f) = \int_b^a f(x)dx - \sum_{i=0}^{n} H_i f(a_i). \tag{2.23}$$

The error of Simpson method can be determined using expression 2.24 [7]

$$E(f) = -\frac{(b-a)}{180} h^4 f^{(4)}(\zeta), \tag{2.24}$$

where $f^{(4)}$ is the fourth derivative of the f function and ζ is a number from the interval $< a, b >$.

2.3 Lagrange interpolation

Lagrange formula is a way to compute a polynomial interpolation of any order for a fixed set of points. The interpolation is given by formula 2.25 [7]

$$L_n(x) = \sum_{i=0}^{n} f(a_i) l_i(x) \tag{2.25}$$

where the factor $l_i(x)$ is given by expression

$$l_i(x) = \frac{(x-a_0)...(x-a_{i-1})(x-a_{i+1})...(x-a_n)}{(a_i-a_0)...(a_i-a_{i-1})(a_i-a_{i+1})...(a_i-a_n)}. \tag{2.26}$$

The error of Lagrange interpolation formula can be computed by equation 2.27 [7]

$$E(x) = \frac{(x-a_0)(x-a_1)...(x-a_n)}{(n+1)!} f^{(n+1)}(\zeta). \tag{2.27}$$

Lagrange interpolation coefficients $l_i(x)$ for a polynomial of third order that will be used later on will then be

$$\begin{aligned} l_0(x) &= \frac{(x-a_1)(x-a_2)(x-a_3)}{(a_0-a_1)(a_0-a_2)(a_0-a_3)} \\ l_1(x) &= \frac{(x-a_0)(x-a_2)(x-a_3)}{(a_1-a_0)(a_1-a_2)(a_1-a_3)} \\ l_2(x) &= \frac{(x-a_0)(x-a_1)(x-a_3)}{(a_2-a_0)(a_2-a_1)(a_2-a_3)} \\ l_3(x) &= \frac{(x-a_0)(x-a_1)(x-a_2)}{(a_3-a_0)(a_3-a_1)(a_3-a_2)} \end{aligned} \tag{2.28}$$

Chapter 3

Solving the BK equation

The Balitsky-Kovchegov equation unfortunately does not have an analytic solution, so it has to be solved numerically such as in [22, 23, 24]. A usual way of solving this equation involves the Simpson method for integration, Lagrange interpolation for acquiring values of $N(r)$ for intermediate positions and Runge-Kutta method for solving the differential equation.

Since both Simpson method and Runge-Kutta method are using grid points and not continuous functions, the initial condition is computed on an equidistant grid with step h. To obtain the next step in rapidity evolution, one must use the RK method and therefore compute the integral

$$\int d\vec{r_1} K^{run}(\vec{r}, \vec{r_1}, \vec{r_2})(N(\vec{r_1}, x) + N(\vec{r_2}, x) - N(\vec{r}, x) - N(\vec{r_1}, x)N(\vec{r_2}, x)). \tag{3.1}$$

This integral depends on the value of $\vec{r}$, that is the dipole distance and position in which we are making the single rapidity step. It is then necessary to compute this integral for every value of $\vec{r}$ on the whole considered interval. To compute this integral, Simpson method was used. That means that for every value of $\vec{r}$, a cycle has been run for the whole interval integrating the function over $\vec{r_1}$, where the value of r_2 was computed according to

$$r_2 = \sqrt{r^2 + r_1^2 - 2rr_1 cos(\theta)} \tag{3.2}$$

where θ is the angle between $\vec{r}$ and $\vec{r_1}$. If the point r_2 does not match exactly one of the grid points on which the values of the initial condition has been computed, it is necessary to interpolate. Lagrange interpolation of first or third order is considered since even values of interpolations order tend to inaccurately interpolate linear regions.

For every point r_1 inside the integral 3.1, another integral over θ has been computed. Theta goes from 0 to 2π but since cosine is an even function, we can simplify this by taking integral over $< 0, \pi >$ instead and multiplying the result by a factor of two.

Once the function is integrated over θ in every point r_1, it is possible to integrate these integrated functions and determine the final integral. This integral can be however split in three separate terms:

$$\begin{aligned} Kernel &= \int d^2\vec{r_1} K^{run}(\vec{r_1}, \vec{r_2}, \vec{r}) \\ Split &= \int d^2\vec{r_1} K^{run}(\vec{r_1}, \vec{r_2}, \vec{r})(N(y, \vec{r_1}) + N(y, \vec{r_2})) \\ Recomb &= \int d^2\vec{r_1} K^{run}(\vec{r_1}, \vec{r_2}, \vec{r})(N(y, \vec{r_1})N(y, \vec{r_2})), \end{aligned} \tag{3.3}$$

which allows us to speed up the Runge-Kutta method as described in the Appendix A. These three terms are then used to compute next step in rapidity evolution and this step is then added to the initial condition in every point of r. Obtained function can go through this process again until the desired rapidity is reached.

To speed up this process, it is useful to create a three-dimensional array in the very beginning of the computation that will hold the values of $K^{run}(\vec{r}, \vec{r_1}, \vec{r_2})$ for every combination of r, r_1 and r_2 so that they don't have to be computed over and over. Same principle was used to hold the values of $r_2(r, r_1, \theta)$.

To determine the values of $\alpha_{run}(r^2)$, equation 1.38 is used on a region, where $r > r_{run}$ holds. The value of r_{run} is chosen so that the total value of $\alpha_{run}(r^2)$ would never exceed the value of 0.7.

For some choices of r, r_1 and θ the value of $K^{run}(\vec{r}, \vec{r_1}, \vec{r_2})$ diverges. It is then necessary to exclude these points from the whole integral, because whereas in continuous integration a diverging singularity does not necessarily mean divergence of the entire integral, in the discrete approximation an infinite value added to the integration sum changes the result significantly.

3.1 The Optimal Setup

To find the optimal setup of parameters that are used throughout the computation, analysis of their influence has been made. For each parameter, it was necessary to find a reasonable ratio between precision and difficulty of the computation. Therefore variation was made for each parameter and the amount of change to the resulting function was studied. The formula 3.4

$$D(r, Y) = \frac{\mid N_{or}(r, y) - N_{new}(r, y) \mid}{N_{or}(r, y)} \tag{3.4}$$

describes such change, where N_{or} is the original resulting function at rapidity y and N_{new} is the newly acquired result with varied parameter.

Variation for the type of method has been done where Runge-Kutta method of fourth order, Ralston method and Euler method have been compared see Fig. 3.1 and Fig.

3.2. We can see that the difference between results obtained by Euler and RK2 method are about twice as high as the difference between RK2 and RK4 methods.

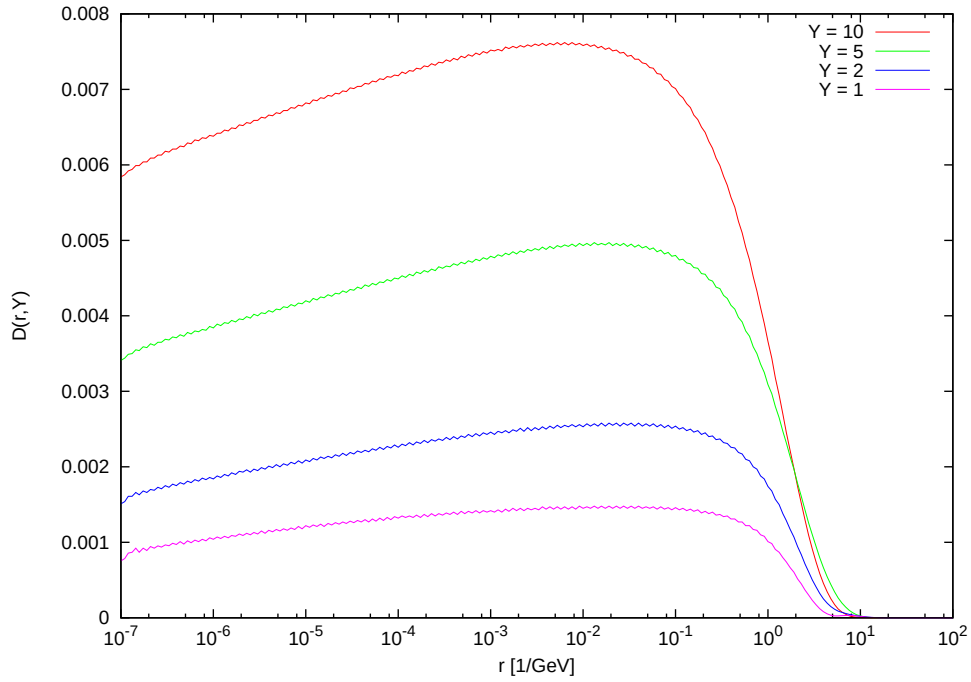

Figure 3.1: A change of the resulting function when Euler method is used instead of Runge-Kutta of second order.

A variation for the integration step over the parameter θ has been done. Steps of 5, 10, 20 and 40 have been compared at various rapidities to determine the optimal speed/precision ratio see Fig. 3.3, 3.4 and 3.5. The change from five steps over the interval of $< 0, \pi >$ to 10 reaches up to 25% for the rapidity of 10 and decreases slowly with rising dipole size r. The change of the resulting function when 20 steps are introduced instead of 10 over $< 0, \pi >$ starts with a value of about 1% for the rapidity of 10 but decreases rapidly with increasing r. As we will see further in the thesis, the low values of r hold a low interest for us because they are not the most influential to the final result. and for the important regions, the change is below the value of 0.1%. When even more steps are introduced, the difference between these functions starts to grow again which may be due to the increasing influence of the rounding error.

A variation over the integration step r has been done. The values of 10, 25, 50 and 100 per order of magnitude were compared as shown in Fig. 3.6, 3.7 and 3.8. We can see that the difference between the result obtained by the method using 10 steps per order of magnitude and 25 steps exceeds the value of 2% on the central part of the interval for the rapidity of 10. This region is particularly important for the precision of the obtained result as shown in following section. When use 50 steps per order of magnitude, the difference between the result obtained with 25 is less than 1% for most of the interval with the exception of values of r smaller then 10^{-6}. The difference when 100 steps per order of magnitude is introduced has also less then 1% difference in that region when compared to the previous 50 steps method.

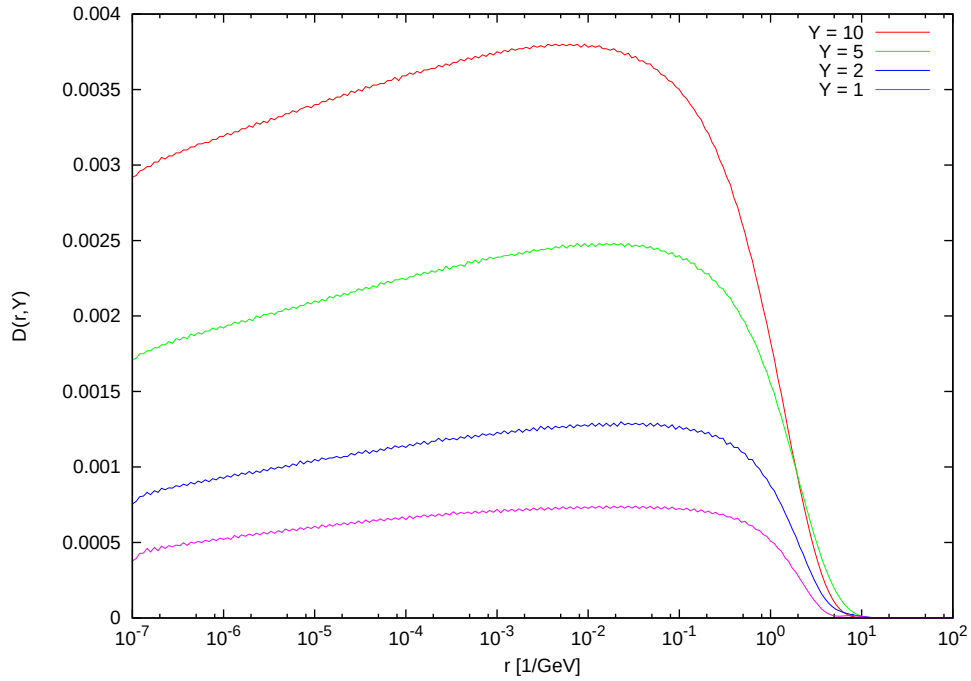

Figure 3.2: A change of the resulting function when Runge-Kutta method of fourth order is used instead of Runge-Kutta of second order.

A various methods of interpolation were carried out. The difference between the initial linear interpolation and Lagrange interpolation of third order is shown in Fig. 3.9. and the actual result functions in Fig. 3.10. As it turns out, the cubic interpolation might not be ideal for this case since it does not very well describe the regions where slope changes rapidly and error is introduced into the evolution. From the figure 3.10, we can see that at some regions, the value of $N(r, y)$ exceeds the value of one, which is a clear error, since its values should always be in the <0,1> interval.

The step of the Runge-Kutta method was also varied. The difference between the step of 0.05 rapidity per step to the step 0.01 is shown inf Fig. 3.11 and the difference between 0.01 and 0.005 steps is shown in Fig. 3.12. Where as the obtained function can differ at about 4% at rapidity of 10 when steps of 0.05 and 0.01 are compared, for further interval splitting (from 0.01 to 0.005) the difference reaches only the value of 0.5% at one point at the rapidity of 10. The dependence of the photon wave function on the step over the parameter z was studied in Fig. 3.13.

A dependence of the evolution was also studied according to the change of the initial conditions. Various initial conditions were evolved using the Balitsky-Kovchegov evolution equation. Runge-Kutta method of fourth order was used for solving the differential equation and Simpson rule was used to compute the integral.

The evolution of a more common initial condition setup is shown in Fig. 3.14. Figure 3.15 shows the evolution for a simple linear initial condition that has a value of 0 for all dipole sizes below 1, linearly grows to one in the (1,10) interval and has a value of 1 elsewhere. Even more extreme initial condition was considered in Figure 3.16,

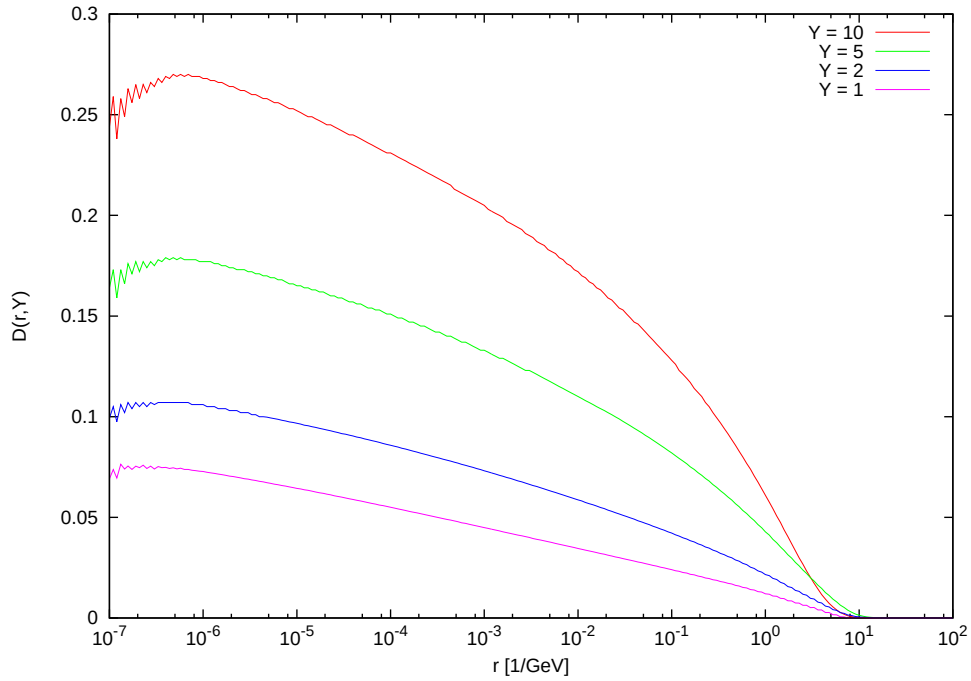

Figure 3.3: A change of the resulting function when 10 steps per interval of θ is considered compared to step of 5.

that shows the evolution for an initial condition that exceeds the unrealistic value of 1 for $N(r, Y)$. It has a value of 0 for r smaller then 1, linearly grows up to the value of 1.5 at the dipole size of twenty, and is set to 1 everywhere else. Final initial condition considered is shown in Fig. 3.17. It does not reach the value of one for $N(r, Y)$ anywhere on the interval and is set to 0 for the dipole sizes smaller than one, grows linearly to the value of 0.5 at $r = 5$ and stays at that value for the remaining part of the interval.

Note that the dipole size axis is in the logarithmic scale. In the regular scale, slope of these initial conditions is not linear.

We can see that these extreme initial conditions seem not to affect the later evolution and that the evolution equation itself shapes the curve into a predetermined shape. In all of these cases we can see that by rapidity of 8, shape of the initial condition is suppressed and that the evolution than continues similarly for all initial conditions.

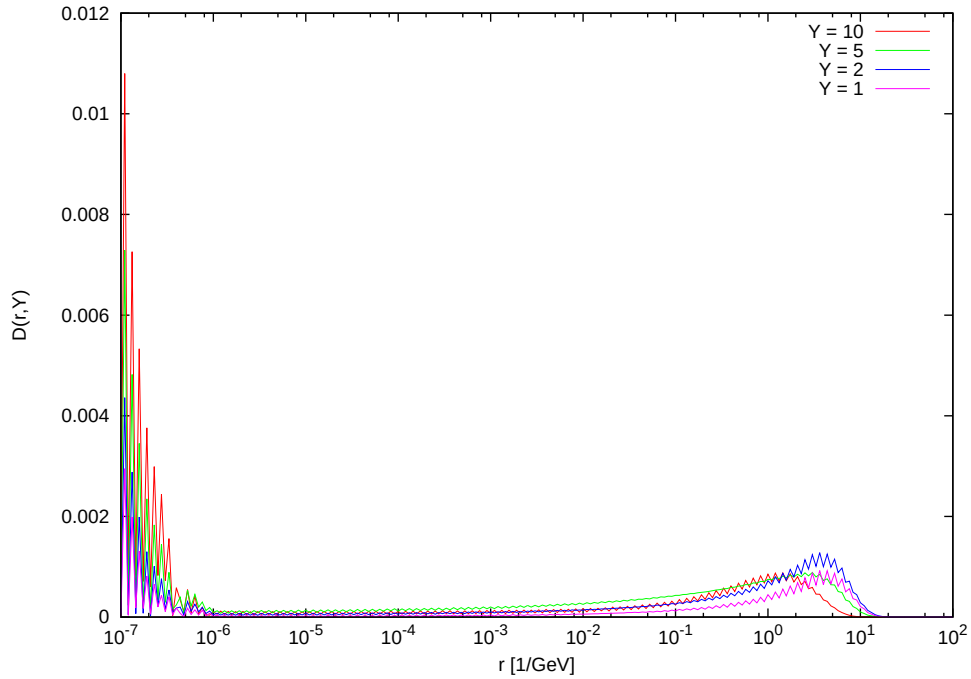

Figure 3.4: A change of the resulting function when 20 steps per interval of θ is considered compared to step of 10.

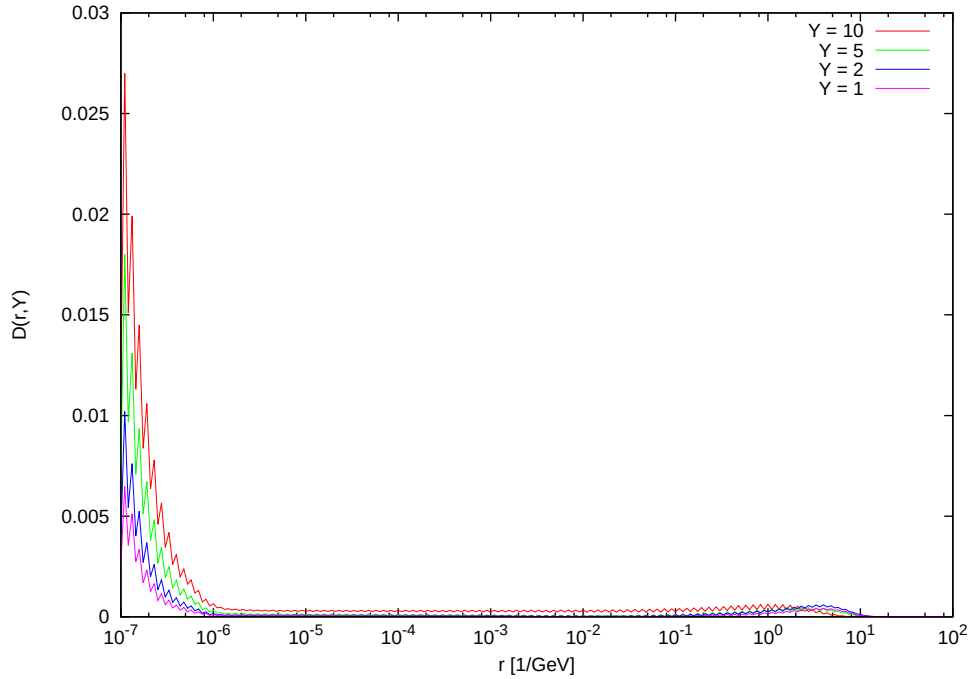

Figure 3.5: A change of the resulting function when 40 steps per interval of θ is considered compared to step of 20.

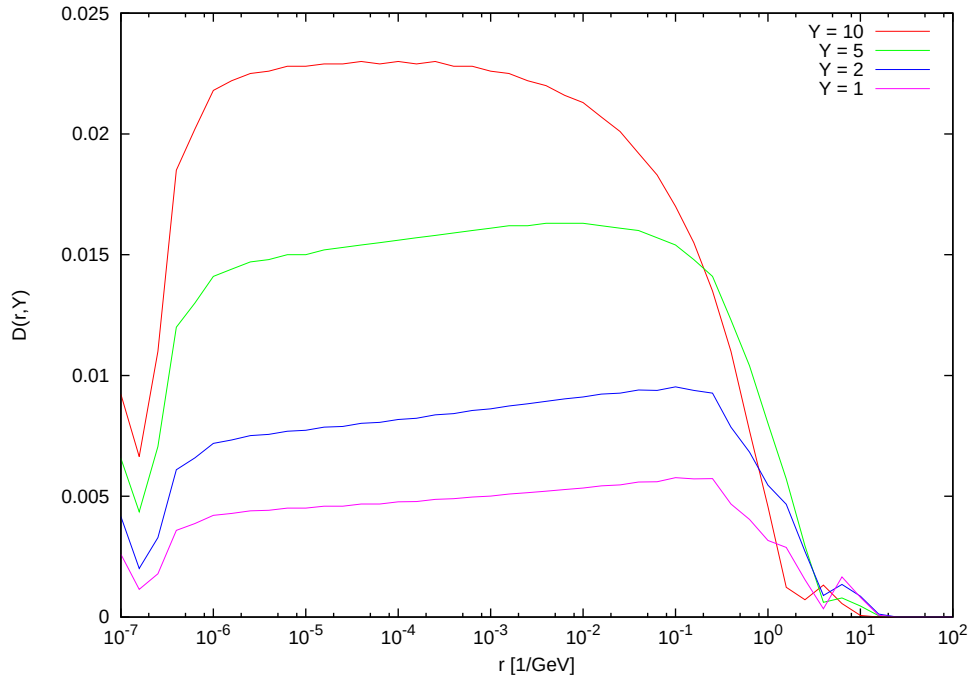

Figure 3.6: A change of the resulting function when 25 steps per order of magnitude is considered compared with 10.

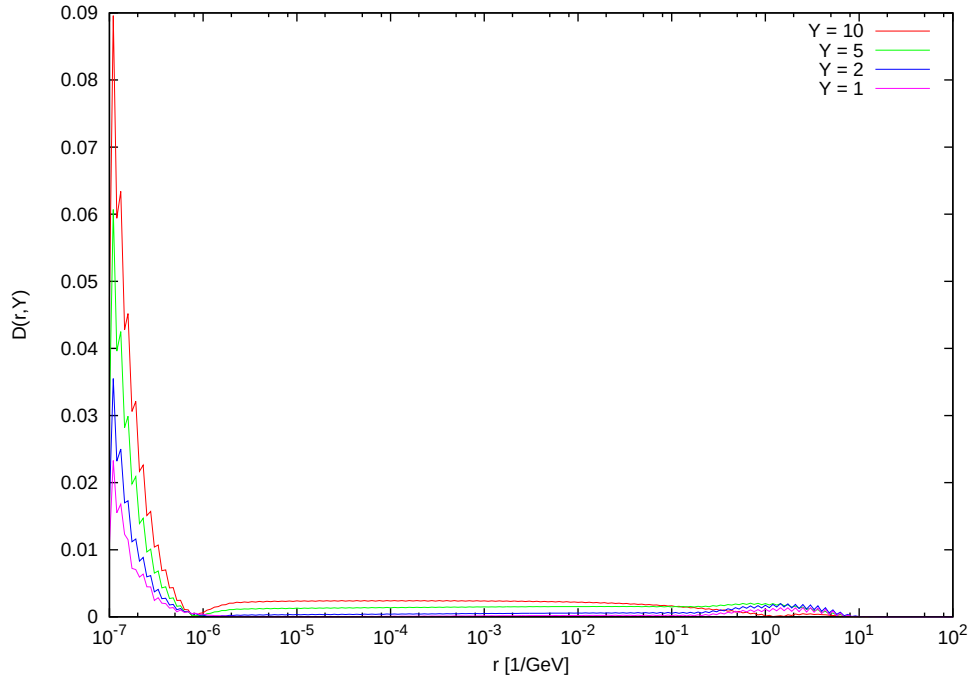

Figure 3.7: A change of the resulting function when 50 steps per order of magnitude is considered compared with 25.

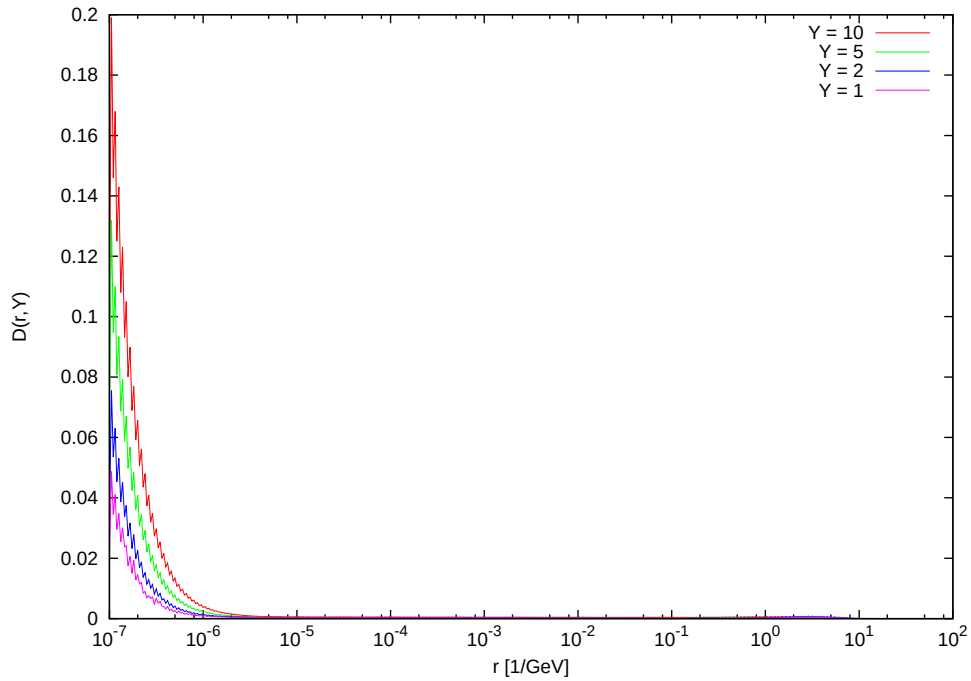

Figure 3.8: A change of the resulting function when 100 steps per order of magnitude is considered compared with 50.

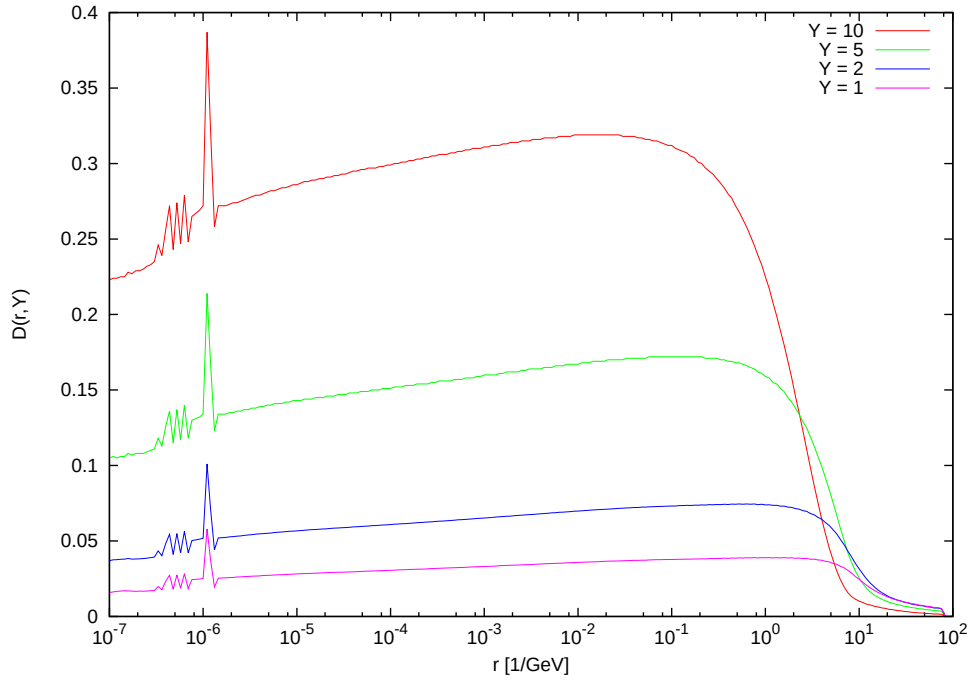

Figure 3.9: A change of the resulting function when Lagrange interpolation of third order is introduced.

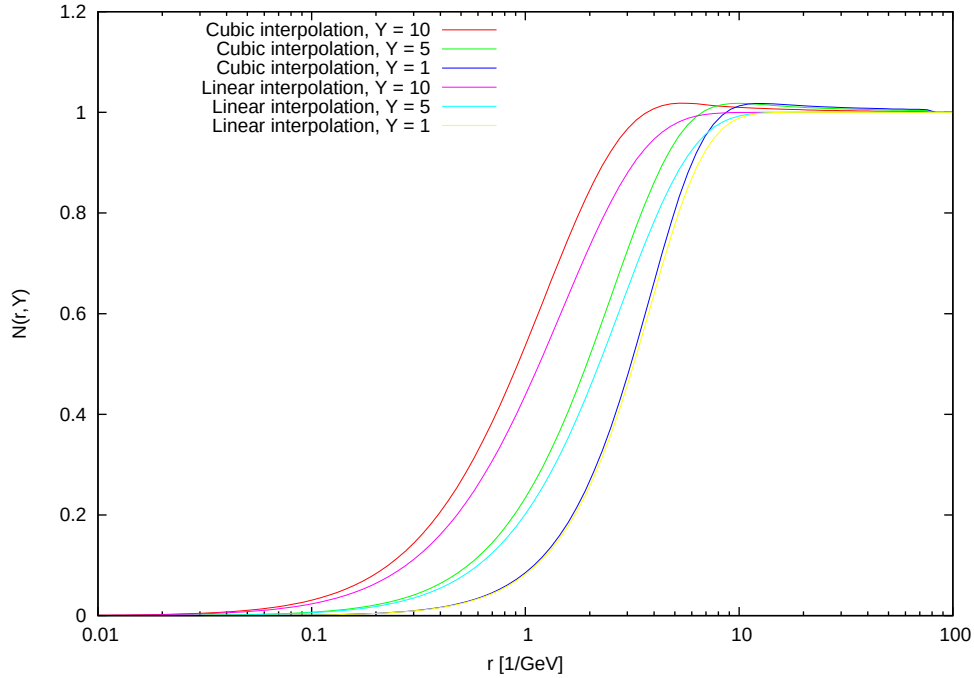

Figure 3.10: A comparison of a linearly interpolated result to the cubic interpolated one.

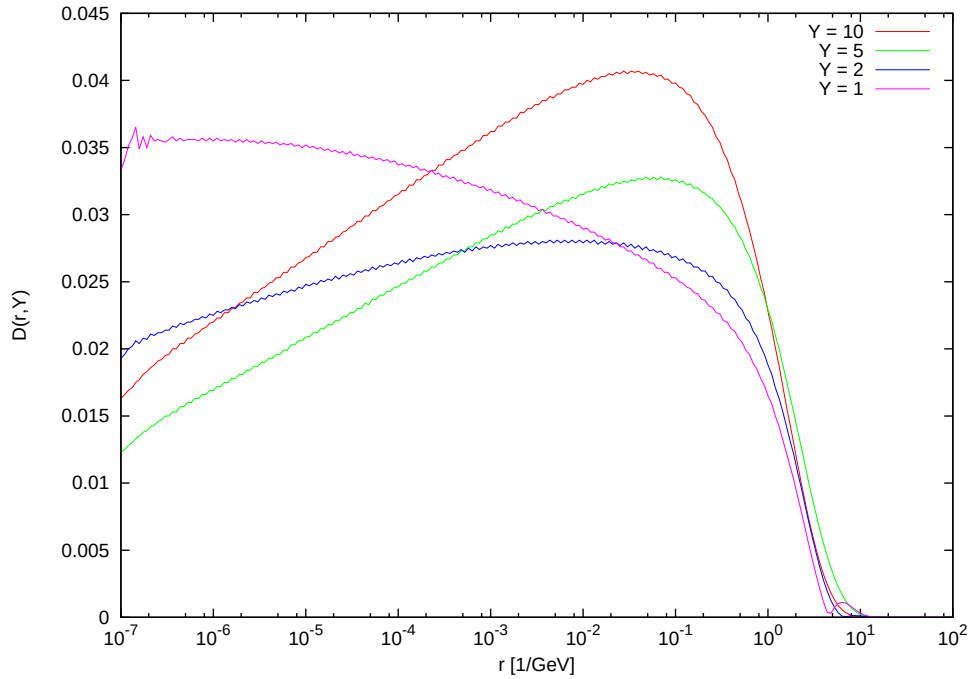

Figure 3.11: A change of the resulting function when step in the Runge-Kutta method is 0.01 compared to the step of 0.05.

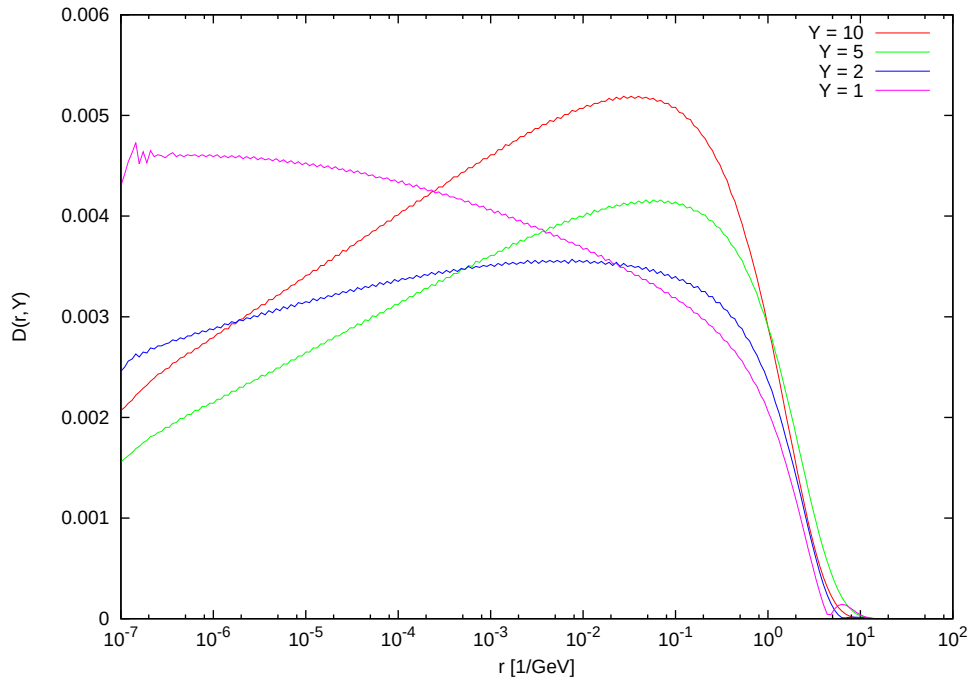

Figure 3.12: A change of the resulting function when step in the Runge-Kutta method is 0.005 compared to the step of 0.01.

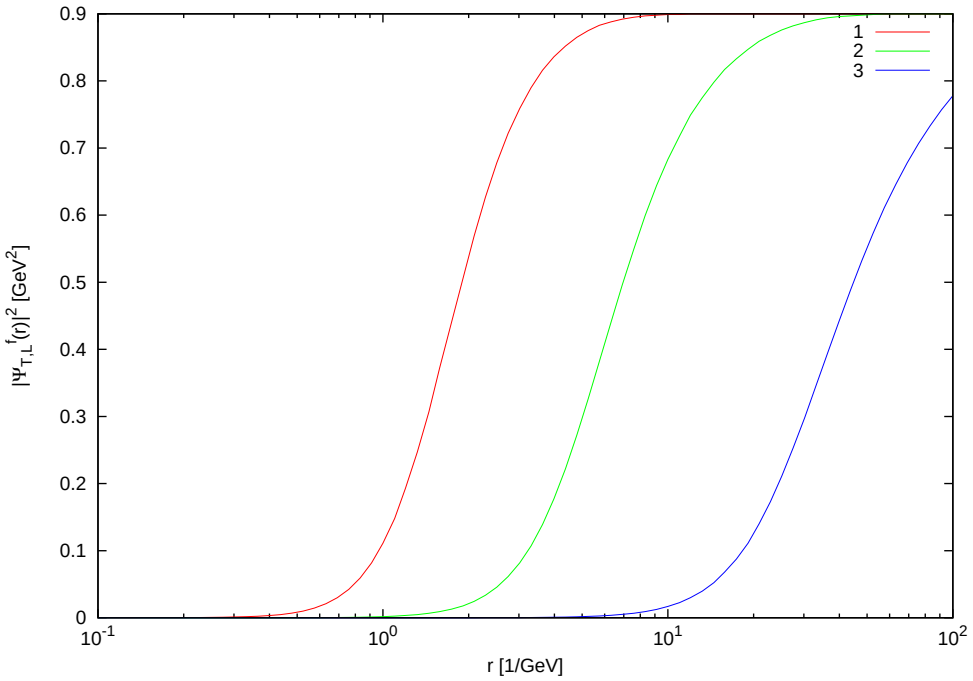

Figure 3.13: A change of the photon wave function when various steps in z are considered. Number 1 shows the change when a step of 10^{-3} is considered instead of 10^{-2}. Number 2 for a change from 10^{-3} to 10^{-4} and number 3 for a change from 10^{-4} to 10^{-5}

.

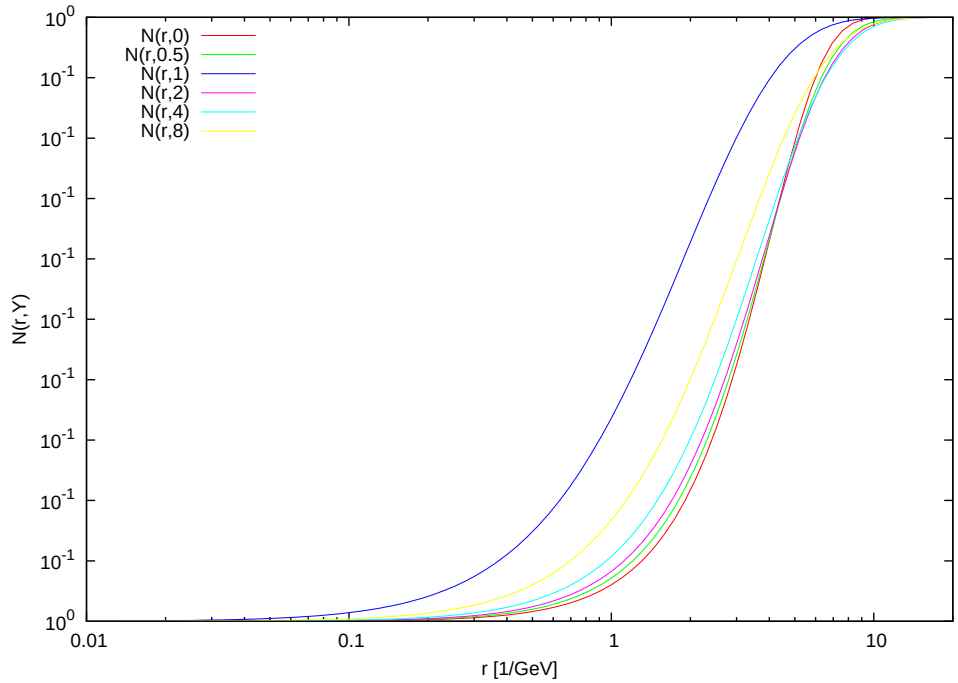

Figure 3.14: Evolution of N(r,Y) for a MV initial condition as described in chapter Balitsky-Kovchegov evolution equation.

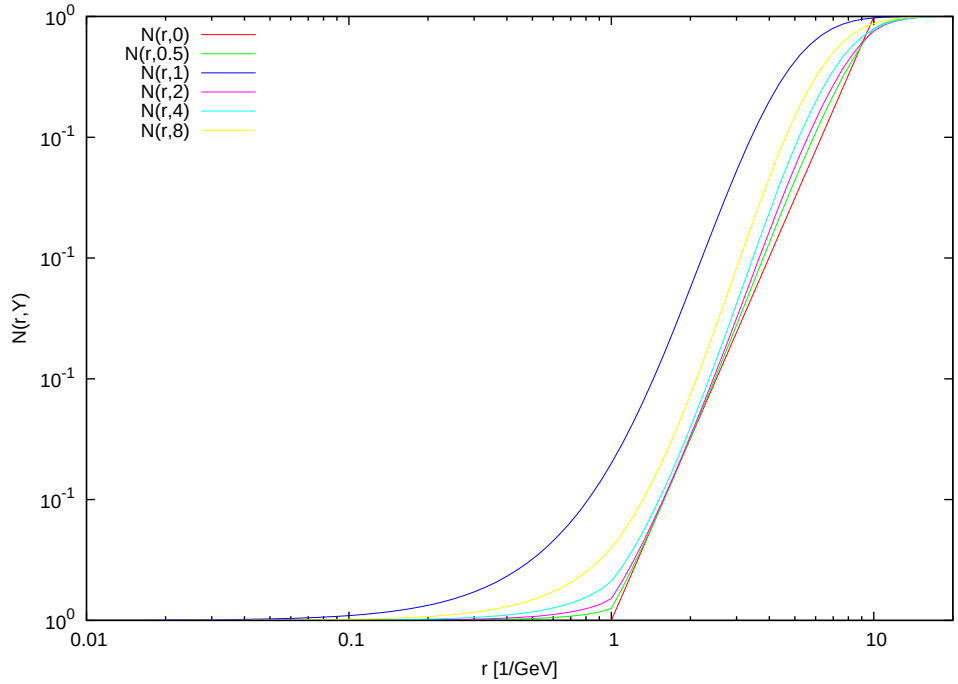

Figure 3.15: Evolution of N(r,Y) when a simple linear initial condition is used.

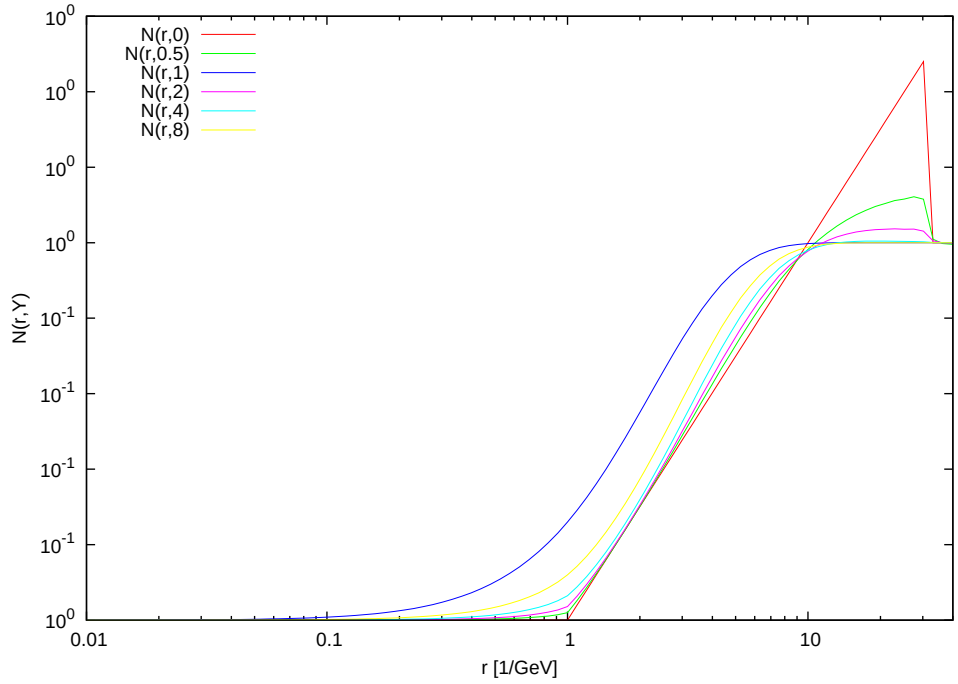

Figure 3.16: Evolution of N(r,Y) when an atypical initial condition is used, that exceeds the value of one.

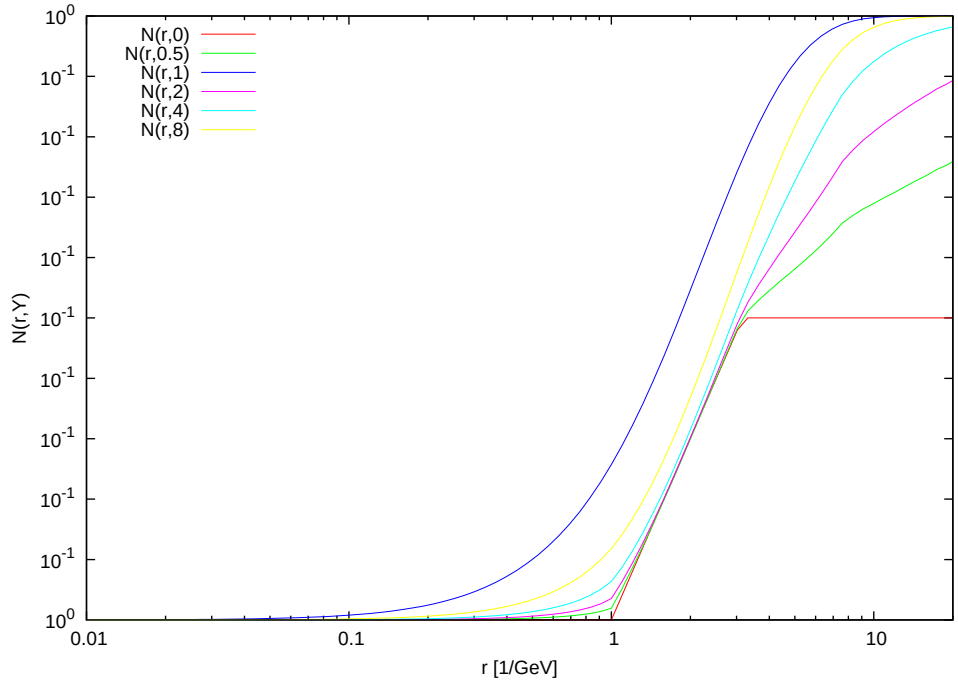

Figure 3.17: Evolution of N(r,Y) when an atypical initial condition is used, that does not reach one.

Chapter 4

Results

A Balitsky Kovchegov evolution equation was used to obtain following results combined with Simpson's rule for integration and Runge-Kutta method of fourth order for solving the differential equation. The optimized implementation of Runge-Kutta method for the special case of the BK evolution equation is described in the Appendix A. The step of rapidity of the RK method was chosen to be 0.01 and there were 25 steps per order of r for the Simpson's rule. There were 20 steps for the interval $< 0, 2\pi >$ of θ. As the initial condition, the MV setup was chosen with parameters set to values as shown in section Balitsky-Kovchegov evolution equation.

The properties of the photon wave function $\mid \psi_{T,L} \mid^2$ weighted with various factors that are needed to compute the proton structure function and reduced cross section are shown in the following figures as well as the evolution of $N(r, Y)$ with respect to rapidity and r. Fig. 4.3 shows the dependence of $\mid \psi_{T,L} \mid^2$ to r for different values of Q^2.

To obtain the structure function $F_2(x, Q^2)$, it is only needed to integrate the function shown in Fig. 4.5 and multiply it by a constant. This function reaches a value of 10^{-8} at $r = 0.01$ GeV^{-1}, which is below its maximum value by a factor of 10^{-4}. Similar situation occurs at $r = 40$ GeV^{-1}. A region of the main interest and desired precision for obtaining an accurate value of $F_2(x, Q^2)$ is then $r \sim (0.1, 30)$ GeV^{-1}.

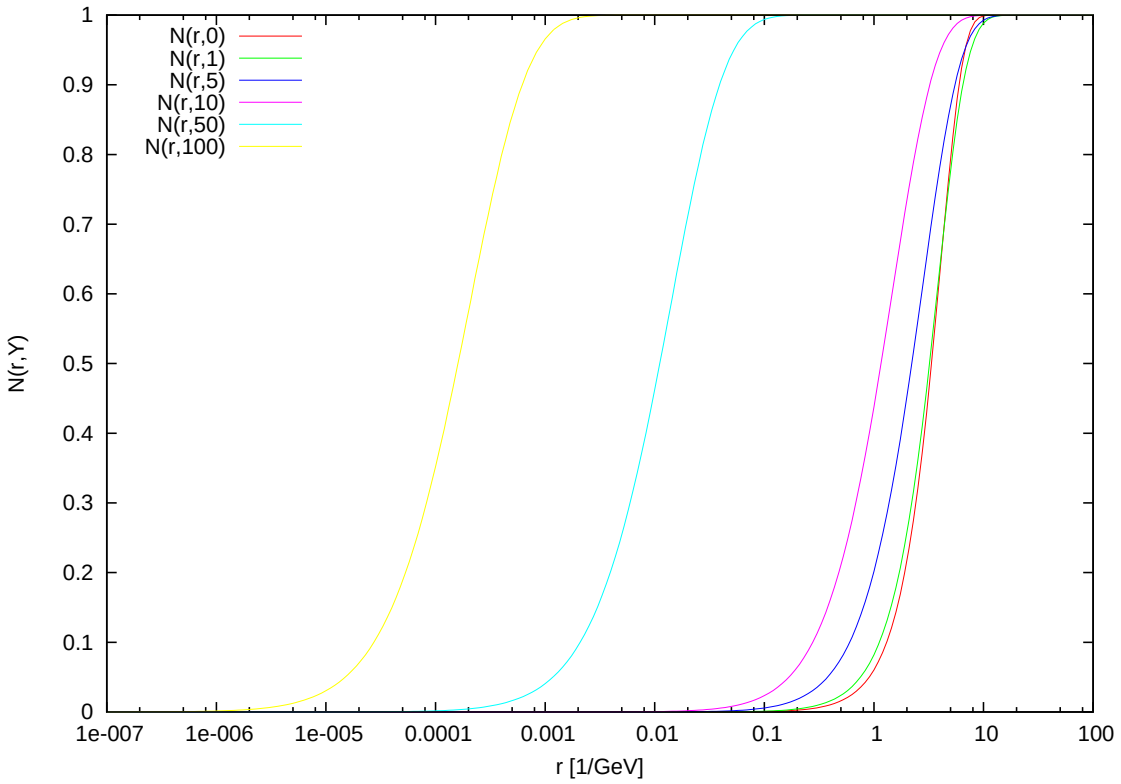

Figure 4.1: The dependence of $N(r, Y)$ on r for various rapidities.

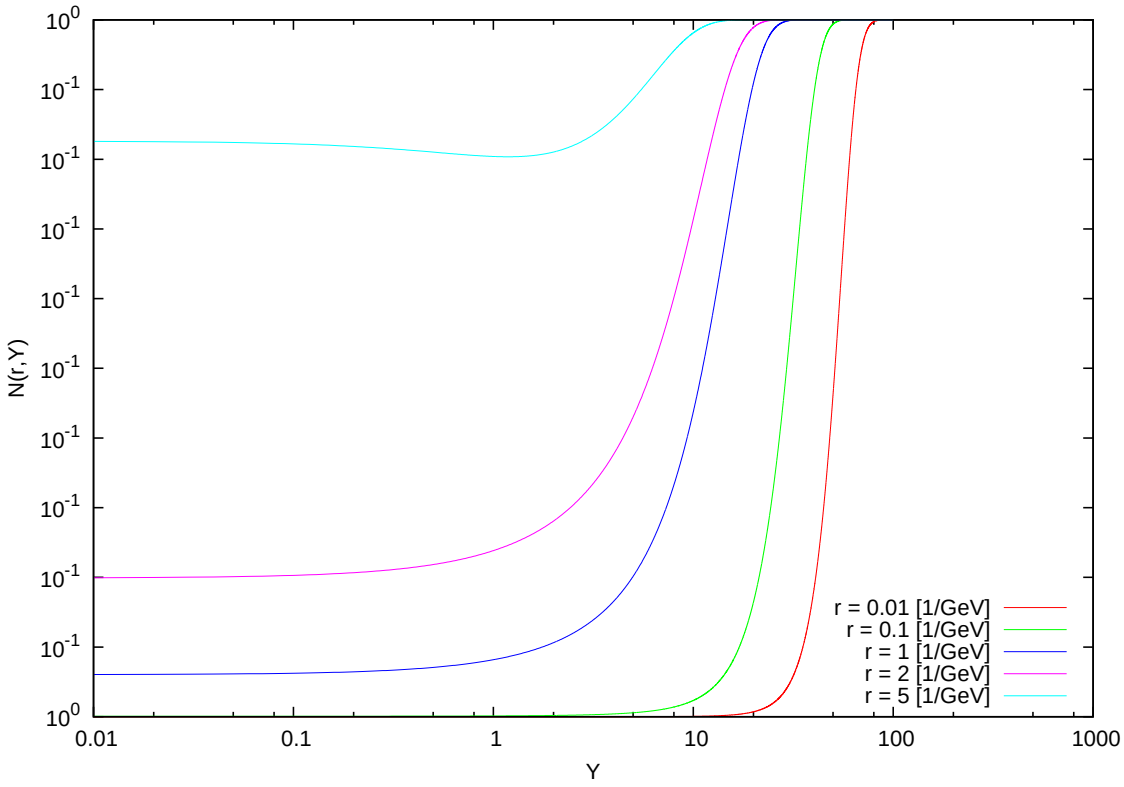

Figure 4.2: The dependence of $N(r, Y)$ on Y for various values of r.

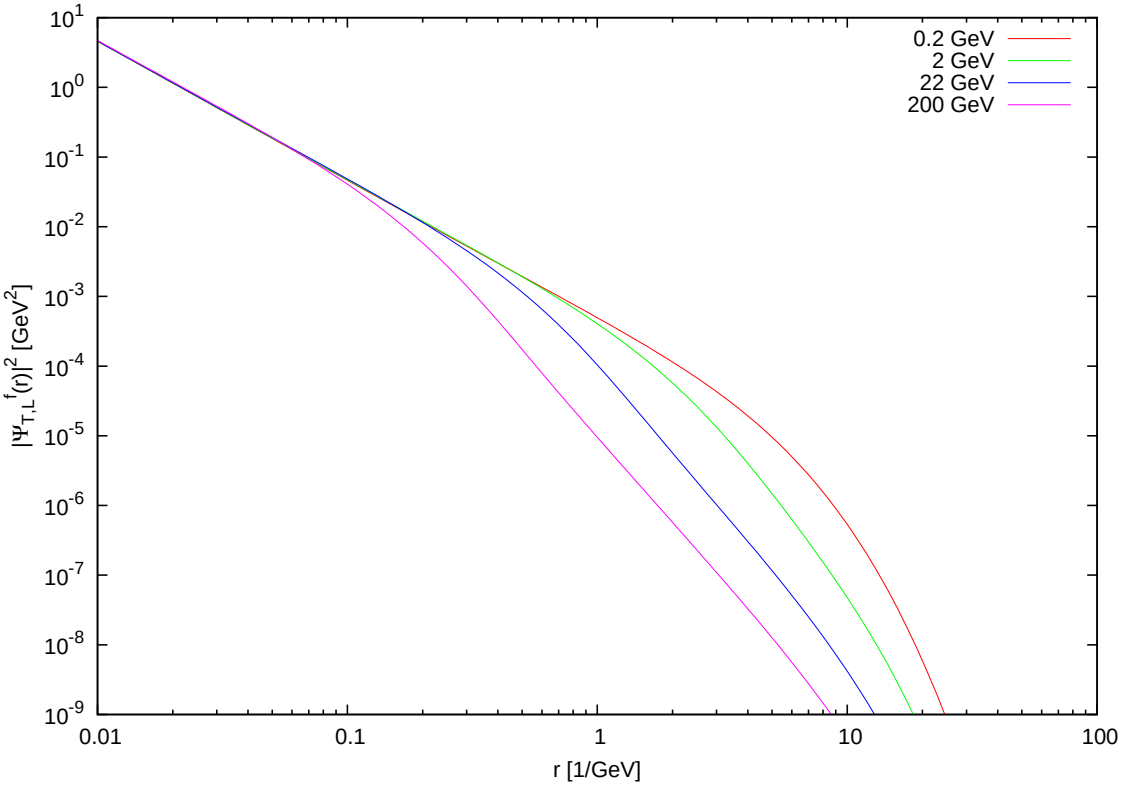

Figure 4.3: The photon wave function $\mid \psi_{T,L} \mid^2$ integrated over z.

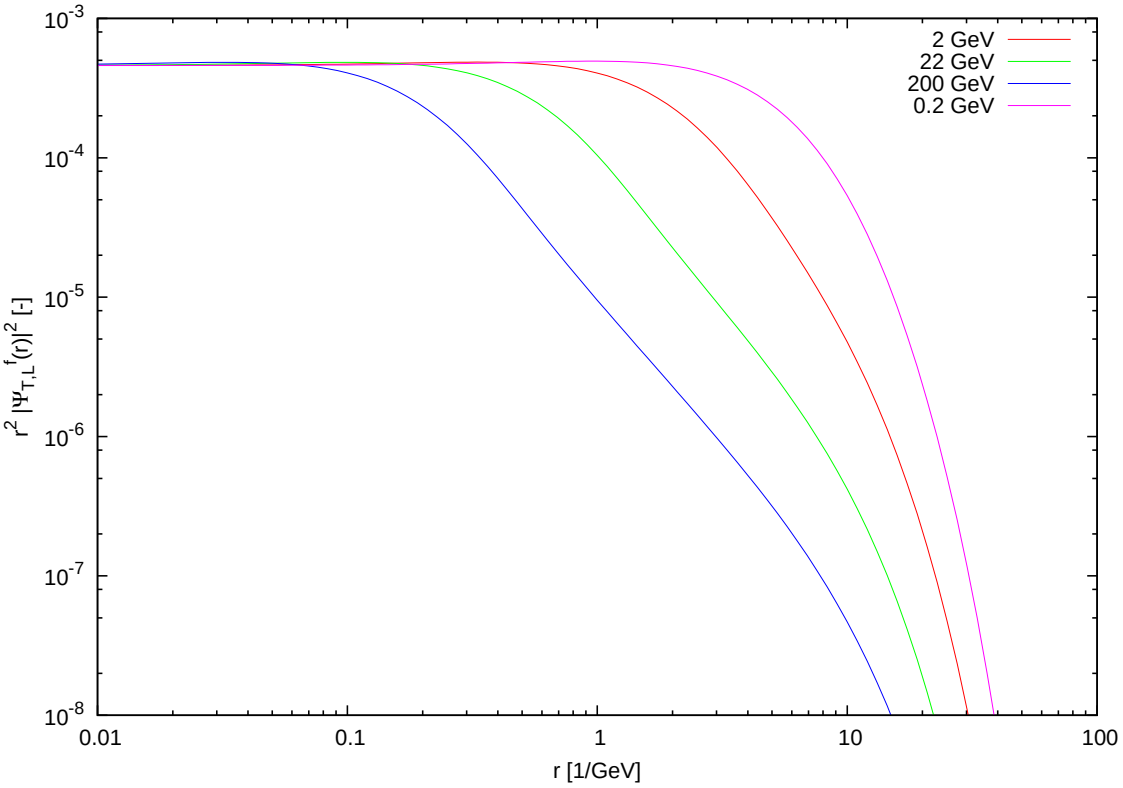

Figure 4.4: $r^2 \mid \psi_{T,L} \mid^2$ integrated over z for various values of Q^2.

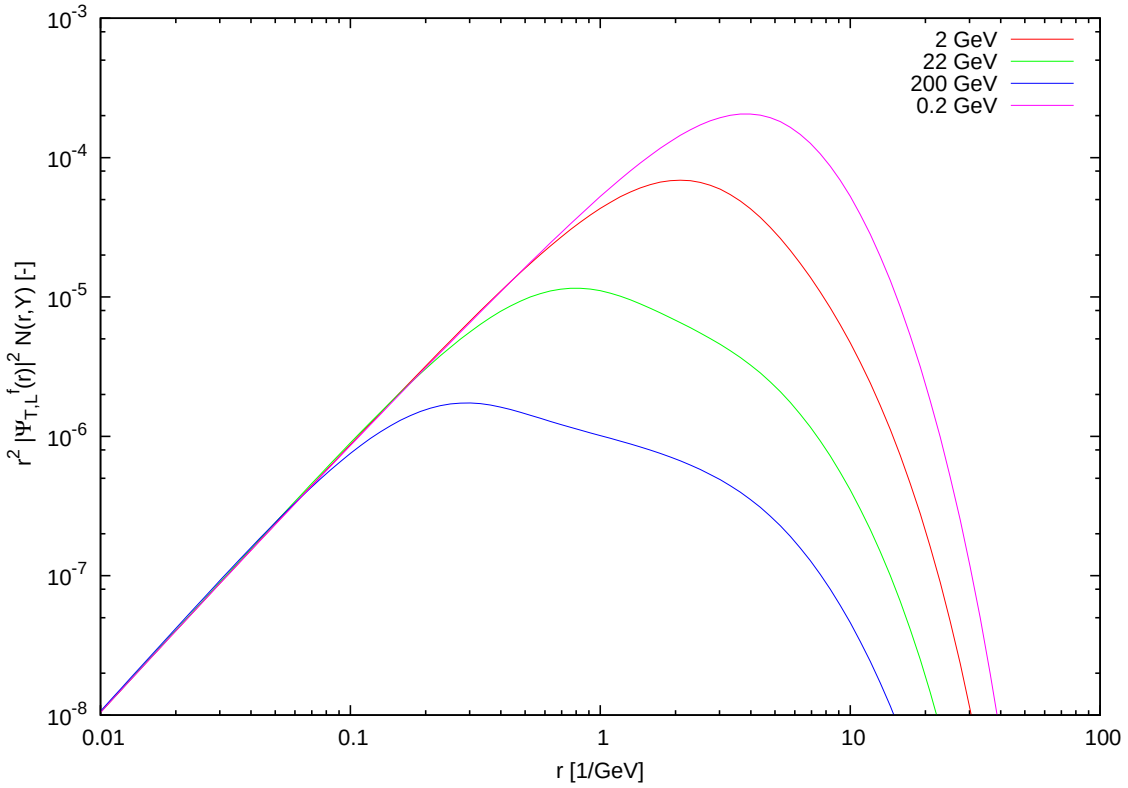

Figure 4.5: The photon wave function $\mid \psi_{T,L} \mid^2$ multiplied by the scattering amplitude $N(r, Y)$ and r^2 for various values of Q^2.

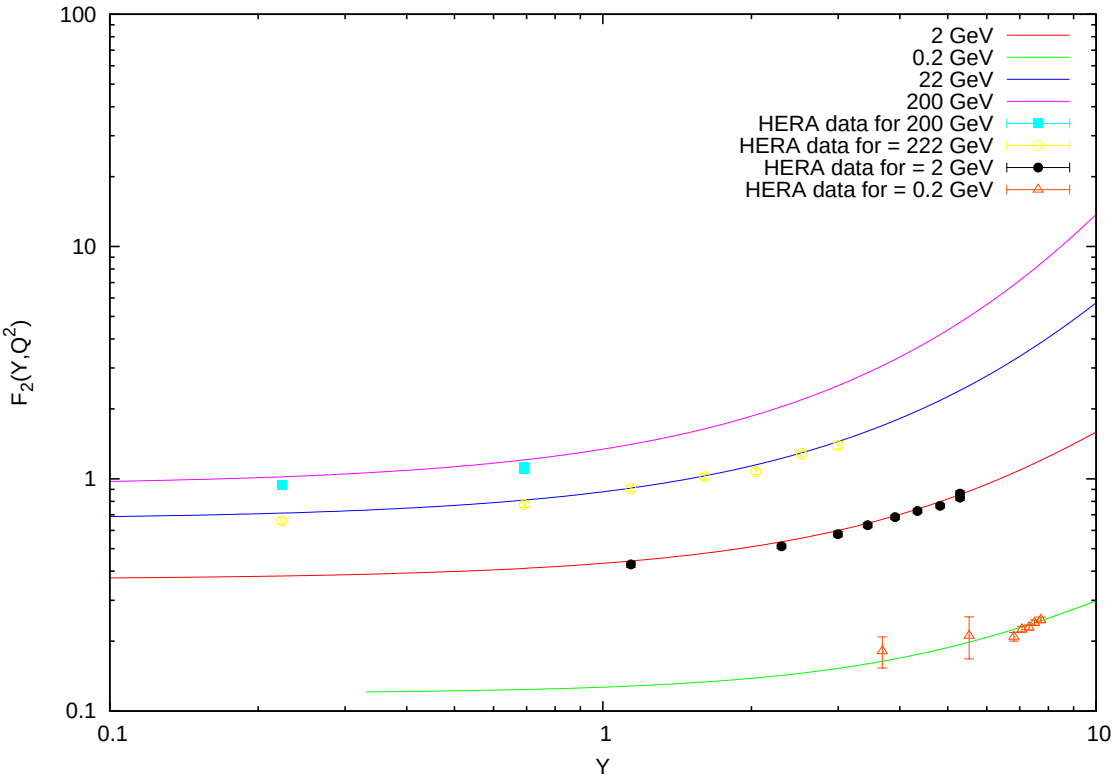

Figure 4.6: The dependence of the proton structure function $F_2(Y, Q^2)$ on Y and compared with data from HERA [31].

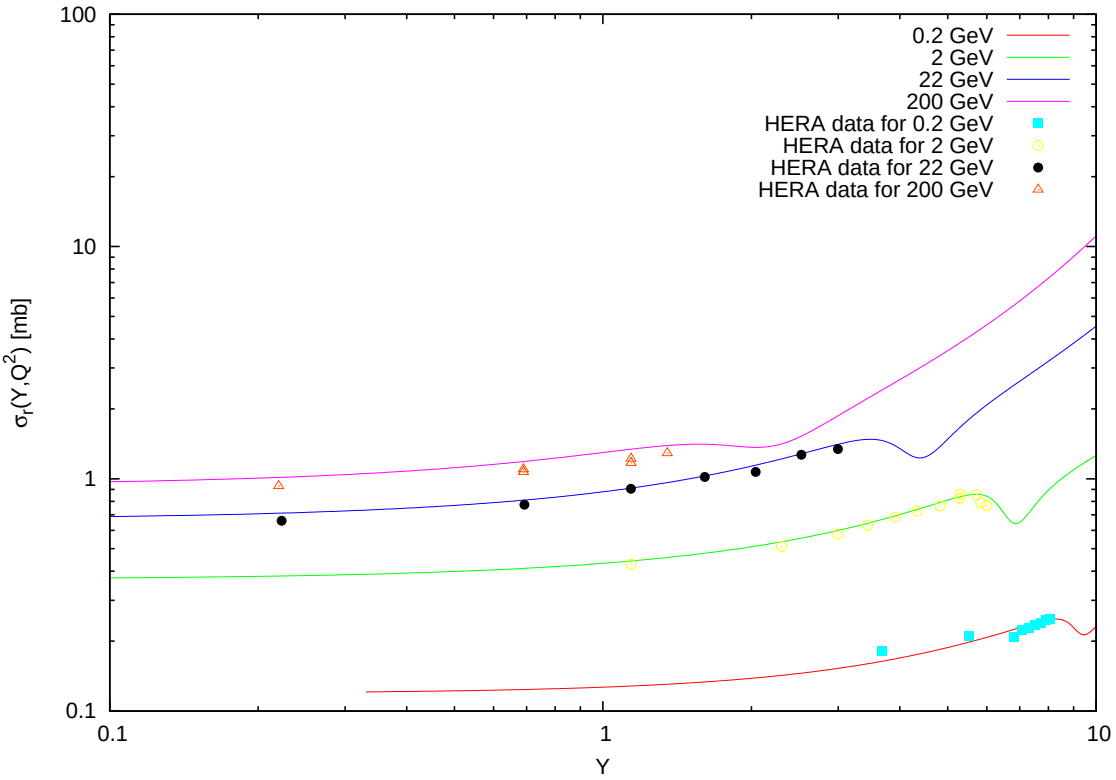

Figure 4.7: The dependence of the reduced cross section $\sigma_r(Y, Q^2)$ on Y compared with data [31].

Conclusion

There are several models that predict the effect of saturation of partons in high energy collisions [20, 21]. Balitsky Kovchegov evolution equation does that by modifying the BFKL equation with recombination processes that occur in hadrons at high energies. These are typically reached in large accelerators such as LHC, HERA or RHIC. Its solution can predict correctly the values of structure functions of hadron or DIS reduced cross section in four orders of Q^2. It is a integro-differential equation and it typically cannot be solved analytically.

Balitsky Kovchegov evolution equation was numerically solved using the Runge-Kutta method of fourth order, Simpson rule and Lagrange interpolation. Various methods were tested and their initial parameters compared to obtain the best ratio of precision and computing speed since the program for solving BK evolution equation is time demanding.

The optimal parameters to compute the BK equation prove to be the Runge-Kutta method of fourth order with a step of 0.01 in rapidity, Simpson rule for the integration with step of 20 over the interval over θ and 25 steps per order of magnitude of the dipole size r. A simple linear interpolation has been determined to give the best results since higher orders are not precise in certain regions and misshape the computed function. For the computation of the photon wave function, 10000 steps per the interval of $< 0, 1 >$ over the parameter z were chosen.

BK equation has been also tested for various initial conditions. The evolution has been carried out for initial conditions with much lower and higher values than those of standard initial condition. The resulting evolution was almost unchanged even with these extreme parameters and the equation "forgot" the initial condition at rapidity of about 8.

The shape of the photon wave functions was calculated and plotted with various factors that also take part in the final structure function computation. It was shown that the strongest effect on the final value of cross section and structure function hold the values for which $r \sim (0.1, 30)$ GeV^{-1} since the photon wave functions weighted by the solution of BK evolution equation show negligible values in those regions and thus do not affect the final integral over r as much. The structure function F_2 and reduced cross section $\sigma_{T,L}$ were computed from the obtained solutions given by BK equation for various values of Q^2 and compared to data acquired by HERA.

Appendix A
Runge Kutta method for the BK equation

If we apply the Runge-Kutta method of fourth order to the Balitsky Kochegov equtaion, the general expression

$$\begin{aligned} N(y+h) &= N(y) + \frac{1}{6}h(k_1 + 2k_2 + 2k_3 + k_4) \\ k_1 &= f(N(y)) \\ k_2 &= f(N(y) + \frac{1}{2}hk_1) \\ k_3 &= f(N(y) + \frac{1}{2}hk_2) \\ k_4 &= f(N(y) + hk_3) \end{aligned} \tag{4.1}$$

gets simplified. If we denote

$$\begin{aligned} Kernel &= \int d\vec{r} K^{run}(\vec{r_1}, \vec{r_2}, \vec{r}) \\ Split &= \int d\vec{r} K^{run}(\vec{r_1}, \vec{r_2}, \vec{r})(N(y, \vec{r_1}) + N(y, \vec{r_2})) \\ Recomb &= \int d\vec{r} K^{run}(\vec{r_1}, \vec{r_2}, \vec{r})(N(y, \vec{r_1})N(y, \vec{r_2})) \end{aligned} \tag{4.2}$$

and

$$f(N(y,r)) = \int d\vec{r_1} K^{run}(\vec{r}, \vec{r_1}, \vec{r_2})(N(\vec{r_1}, x) + N(\vec{r_2}, x) - N(\vec{r}, x) - N(\vec{r_1}, x)N(\vec{r_2}, x)) \tag{4.3}$$

then we can express the Runge Kutta coefficients as

$$k_1 = f(N(y)) \tag{4.4}$$

$$
\begin{aligned}
k_2 = f(N(y) + \frac{1}{2}hk_1) = \int d\vec{r_1} K^{run}(\vec{r}, \vec{r_1}, \vec{r_2})(N(\vec{r_1}, x) + N(\vec{r_2}, x) - \\
N(\vec{r}, x) + \frac{1}{2}hk_1 - (N(\vec{r_1}, x) + \frac{1}{2}hk_1)(N(\vec{r_2}, x) + \frac{1}{2}hk_1)) \\
= k_1 + \frac{1}{2}hk_1 Kernel - \frac{1}{2}hk_1 Split - \frac{1}{4}h^2 k_1^2 Kernel
\end{aligned} \tag{4.5}
$$

$$
k_3 = f(N(y) + \frac{1}{2}hk_2) = k_1 + \frac{1}{2}hk_2 Kernel - \frac{1}{2}hk_2 Split - \frac{1}{4}h^2 k_2^2 Kernel \tag{4.6}
$$

$$
k_4 = f(N(y) + hk_3) = k_1 + \frac{1}{2}hk_3 Kernel - \frac{1}{2}hk_3 Split - \frac{1}{4}h^2 k_3^2 Kernel \tag{4.7}
$$

Which allows us to speed up the whole method since after the initial computation of $Kernel$, $Split$ and $f(N(y))$, there is no need to integrate the whole function again for obtaining the Runge-Kutta coefficients of higher order.

Bibliography

[1] MANTYSAARI, H.: *Balitsky-Kovchegov equation.* University of Jyvaskyla, 2011.

[2] ALBACETE, J. L.; MARQUET, C.: *Gluon saturation and initial conditions for relativistic heavy ion collisions.* Centre de Physique Thseorique, Ecole Polytechnique, CNRS, 91128 Palaiseau, France, 2014.

[3] OLIVEIRA, E.G.; *Balitsky–Kovchegov evolution equation.* Universidade Federal do Rio Grande do Sul [online] 2009 [cit. 17.3.2015] Available on: <http://www.if.ufrgs.br/gfpae/sem/2008/BK.pdf>.

[4] MCLERRAN, L.:*The CGC and the Glasma: Two Lectures at the Yukawa Insitute.* Physics Department and Riken Brookhaven Center, Brookhaven National Laboratory, 2010.

[5] ALBACETE, J. L.; ARMESTO, N.; MILHANO, J. G.; ARIAS, P. Q.; SALGADO, A. C.: *AAMQS: A non-linear QCD analysis of new HERA data at small-x including heavy quarks.* CERN-PH-TH 2010-314.

[6] IANCU, E.; TRIANTAFYLLOPOULOS, D. N.: *JIMWLK evolution: From color charges to rapidity correlations* Nuclear Physics A, 932, (2014), 63–68.

[7] VITASEK, E.: *Numericke metody* SNTL, 428,Praha 1987.

[8] *Eulerova metoda.* University of Zagreb [online] 2001 [cit. 19.3.2015] Available on: <http://master.grad.hr/nastava/matematika/mat3/node161.html>.

[9] *PHYS 580 COMPUTATIONAL PHYSICS* . San Diego state University [online] 2014 [cit. 20.3.2015] Available on: <http://www.physics.sdsu.edu/ johnson/phys580/rk1.jpg>.

[10] KOVCHEGOC, Y. V.: *Brief Review of Saturation Physics.* Department of Physics, The Ohio State University, Columbus, 2014.

[11] KUHLEN, M.: *QCD at HERA The Hadronic Final State in Deep Inelastic Scattering.* Springer Tracts in Modern Physics Vol. 150, 1999.

[12] K. J. Golec-Biernat and M. Wusthoff: *Saturation effects in deep inelastic scattering at low Q^2 and its implications on diffraction.* Phys.Rev. D59 (1998) 014017, [hep-ph/9807513].

[13] I. Balitsky: *Quark contribution to the small-x evolution of color dipole.* Phys.Rev. D75 (2007) 014001, [hep-ph/0609105].

[14] Y. V. Kovchegov and H. Weigert: *Triumvirate of Running Couplings in Small-x Evolution.* Nucl.Phys. A784 (2007) 188?226, [hep-ph/0609090].

[15] E. Predazzi and V. Barone: *High-Energy Particle Diffraction*1 ed., 2002. ISBN 978-3540421078.

[16] L. D. McLerran and R. Venugopalan: Phys. Lett. B424, 15 (1998), nucl-th/9705055.

[17] V. S. Fadin, E. Kuraev, and L. Lipatov: *On the Pomeranchuk Singularity in Asymptotically Free Theories.* Phys.Lett. B60 (1975) 50?52.

[18] L. Lipatov: *Reggeization of the Vector Meson and the Vacuum Singularity in Nonabelian Gauge Theories.* Sov.J.Nucl.Phys. 23 (1976) 338?345.

[19] E. A. Kuraev, L. N. Lipatov, and V. S. Fadin: *Multi - Reggeon Processes in the Yang-Mills Theory.* Sov.Phys.JETP 44 (1976) 443?450.

[20] Y. V. Kovchegov: *Small x F(2) structure function of a nucleus including multiple pomeron exchanges* Phys.Rev. D60 (1999) 034008, [hep-ph/9901281].

[21] Y. V. Kovchegov: *Unitarization of the BFKL pomeron on a nucleus.* Phys.Rev. D61 (2000) 074018, [hep-ph/9905214].

[22] J. L. Albacete and Y. V. Kovchegov: *Solving high energy evolution equation including running coupling corrections.* Phys.Rev. D75 (2007) 125021, [arXiv:0704.0612].

[23] J. L. Albacete, N. Armesto, J. G. Milhano, and C. A. Salgado: *Non-linear QCD meets data: A Global analysis of lepton-proton scattering with running coupling BK evolution,.* Phys.Rev.D80 (2009) 034031, [arXiv:0902.1112].

[24] J. L. Albacete, N. Armesto, J. G. Milhano, P. Quiroga-Arias, and C. A. Salgado: *AAMQS: A non-linear QCD analysis of new HERA data at small-x including heavy quarks.* Eur.Phys.J. C71 (2011) 1705, [arXiv:1012.4408].

[25] J. Jalilian-Marian, A. Kovner, A. Leonidov, and H. Weigert: *The Wilson renormalization group for low x physics: Towards the high density regime.* Phys.Rev. D59 (1998) 014014, [hep-ph/9706377].

[26] J. Jalilian-Marian, A. Kovner, and H. Weigert: *The Wilson renormalization group for low x physics: Gluon evolution at finite parton density.* Phys.Rev. D59 (1998) 014015, [hep-ph/9709432].

[27] H. Weigert: *Unitarity at small Bjorken x.* Nucl.Phys. A703 (2002) 823?860, [hep-ph/0004044].

[28] E. Iancu, A. Leonidov, and L. D. McLerran: *Nonlinear gluon evolution in the color glass condensate.* 1., Nucl.Phys. A692 (2001) 583?645, [hep-ph/0011241].

[29] E. Iancu, A. Leonidov, and L. D. McLerran: *The Renormalization group equation for the color glass condensate*. Phys.Lett. B510 (2001) 133?144, [hep-ph/0102009].

[30] E. Ferreiro, E. Iancu, A. Leonidov, and L. McLerran: *Nonlinear gluon evolution in the color glass condensate. 2.Nucl.Phys* . A703 (2002) 489?538, [hep-ph/0109115].

[31] H1 and ZEUS collaborations: *Combined measurement and QCD analysis of the inclusive $e^{\pm}p$ scattering cross sections at HERA* JHEP01 (2010) 109, [arXiv: 0911.0884].

[32] E. Iancu and D.N. Triantafyllopoulos: *JIMWLK evolution in the Gaussian approximation* arXiv:1112.1104v2 [hep-ph] 23 Mar 2012.